Monthly Notices
of the
ROYAL ASTRONOMICAL SOCIETY

MNRAS **452,** 1089–1104 (2015) doi:10.1093/mnras/stv1295

Causality and stability of cosmic jets

Oliver Porth[1,2]★ and Serguei S. Komissarov[1,3]★

[1]*Department of Applied Mathematics, The University of Leeds, Leeds LS2 9JT, UK*
[2]*Centre for Mathematical Plasma Astrophysics, Department of Mathematics, KU Leuven, Celestijnenlaan 200B, B-3001 Leuven, Belgium*
[3]*Department of Physics and Astronomy, Purdue University, West Lafayette, IN 47907-2036, USA*

Accepted 2015 June 7. Received 2015 May 27; in original form 2014 August 18

ABSTRACT

In stark contrast to their laboratory and terrestrial counterparts, cosmic jets appear to be very stable. They are able to penetrate vast spaces, which exceed by up to a billion times the size of their central engines. We propose that the reason behind this remarkable property is the loss of causal connectivity across these jets, caused by their rapid expansion in response to fast decline of external pressure with the distance from the 'jet engine'. In atmospheres with power-law pressure distribution, $p_{\rm ext} \propto z^{-\kappa}$, the total loss of causal connectivity occurs, when $\kappa > 2$ – the steepness which is expected to be quite common for many astrophysical environments. This conclusion does not seem to depend on the physical nature of jets – it applies both to relativistic and non-relativistic flows, both magnetically dominated and unmagnetized jets. In order to verify it, we have carried out numerical simulations of moderately magnetized and moderately relativistic jets. The results give strong support to our hypothesis and provide with valuable insights. In particular, we find that the z-pinched inner cores of magnetic jets expand slower than their envelopes and become susceptible to instabilities even when the whole jet is stable. This may result in local dissipation and emission without global disintegration of the flow. Cosmic jets may become globally unstable when they enter flat sections of external atmospheres. We propose that the Fanaroff–Riley (FR) morphological division of extragalactic radio sources into two classes is related to this issue. In particular, we argue that the low power FR-I jets become reconfined, causally connected and globally unstable on the scale of galactic X-ray coronas, whereas more powerful FR-II jets reconfine much further out, already on the scale of radio lobes and remain largely intact until they terminate at hotspots. Using this idea, we derived the relationship between the critical jet power and the optical luminosity of the host galaxy, which is in a very good agreement with the observations.

Key words: instabilities – MHD – relativistic processes – stars: jets – galaxies: active – galaxies: jets.

1 INTRODUCTION

Collimated outflows (jets) from stars and active galactic nuclei (AGN) are intriguing cosmic phenomena which remain subject of intensive observational and theoretical study since the day of their discovery. In spite of the tremendous progress both in observations and theory, we are still some way from solid understanding of their physics. One of the most remarkable properties of cosmic jets is their ability to keep structural integrity over huge distances. Consider for example jets from young stars. They are traced up to distances of few parsecs and their initial radius, which should be about the size of their central engine, is somewhere between the stellar radius of $\simeq 2\,{\rm R}_\odot$ and 0.1–10 au, depending on the engine model (Ray 2012). Thus, stellar jets cover the distances of order 10^5 or 10^7 of initial radii. The data for AGN jets are even more impressive. Assuming that they are powered by the Blandford–Znajek mechanism (Blandford & Znajek 1977), the initial jet radius is comparable to the gravitational radius of the black hole. For the typical value of the black hole mass, $10^9\,{\rm M}_\odot$, this is $r_{\rm i} \sim 10^{14}$ cm. These jets can be traced up to the distances of hundreds kiloparsecs, which is about one billion(!) initial radii. None of the jets produced in laboratories using most sophisticated jet engines comes even close to their cosmic counterparts in terms of their 'survival' abilities. They lose integrity and get destroyed by dynamic instabilities on much smaller scales, no more than a hundred of initial jet radii.

This remarkable apparent stability of cosmic jets has attracted a lot of attention from theorists, resulting in a very long list of analytical and numerical studies. A comprehensive review of these studies is beyond the scope of this introduction, for this we refer the interested reader to the recent reviews by Hardee (2011) and Perucho (2012). Here we only outline some key concepts and results.

★ E-mail: o.porth@leeds.ac.uk (OP); serguei@maths.leeds.ac.uk (SSK)

Most analytical and numerical studies of jet stability are focused on flows with cylindrical geometry, because they are easier to analyse. The main instabilities in such flows are (1) *Kelvin–Helmholtz (KH) instability* where the source of energy for unstable modes is the bulk motion of the flow (e.g. Birkinshaw 1991) and (2) *magnetic instabilities* which utilize the energy of the jet magnetic field. The latter are similar to those encountered in the experiments on magnetic confinement of plasma (Bateman 1978). The magnetic instabilities are important as most astrophysical jets are believed to be produced via a magnetic mechanism.

In a static column, ideal[1] magnetohydrodynamics (MHD) instabilities are often classified as either *current driven* (CD) where the quantity $\boldsymbol{j}\cdot\boldsymbol{B_0}$ determines the outcome, or *pressure driven* (PD) where $\nabla p_o \approx \boldsymbol{j}\times\boldsymbol{B_0}$ is important (see e.g. Freidberg 1982). In a magnetized flow, the separation between the KH and magnetic instabilities is not that rigid as they can mix and give rise to a new phenomenon (e.g. Baty & Keppens 2002).

Whatever the nature of the instability is, the most disruptive mode is the kink mode ($|m| = 1$), which leads to a displacement of the centre of mass in the jet cross-section. It is recognized that the kink mode can come in two forms – the internal one, where the jet boundary is fixed (e.g. due to a rigid wall) and the external one where it is perturbed as well. Only the latter one is a danger for the jet integrity. In the astrophysical context, the internal mode can actually be beneficial, leading to dissipation required by observations.

Linear stability analysis of cylindrical MHD jets shows that they are generically unstable to the kink mode. Various factors have been shown to influence the growth rate: jet Mach number, density of external medium, velocity shear in the jet, magnetic structure, relativistic effects etc., but none seems to lead to full stabilization under conditions appropriate for astrophysical jets (Hardee & Rosen 2002; Hardee & Hughes 2003; Mizuno, Hardee & Nishikawa 2007). However, the mere fact that a jet is linearly unstable does not necessary mean that it will be completely destroyed by the instability. Its growth may saturate at non-linear phase rather early and result only in mild deformations. Numerical simulations are normally required to handle the non-linear phase and give insight on the saturation regime. In most numerical studies so far, the kink instability shows to be highly disruptive. However, for force-free magnetic configurations the non-linear growth rate can be relatively low (e.g. O'Neill, Beckwith & Begelman 2012). These configurations require poloidal magnetic field comparable to the azimuthal one, which is not feasible at large distances from the jet source. Near the source the poloidal magnetic field may provide the required stability, as indicated by the numerical simulations (McKinney & Blandford 2009; Porth 2013).

Outflows from neutron stars and black holes can be highly magnetically dominated, with magnetic energy density significantly exceeding that of the rest-mass energy of plasma. In the limit of zero inertia of plasma, the equations of relativistic MHD reduce to that of magnetodynamics (MD), where plasma influences the dynamics of electromagnetic field only via perfect conductivity (Komissarov 2002). Analytical studies of MD cylindrical jets concluded that under some conditions they can be stable. In particular, Istomin & Pariev (1994) demonstrated stability to internal kink mode in a jet with uniform axial magnetic field ($B_z = \text{const}$), and Lyubarskii (1999) showed that an unbounded flow is stable if B_z does not decrease outwards. Narayan, Li & Tchekhovskoy (2009) considered quasi-cylindrical equilibrium with an extra term accounting for finite curvature of magnetic surfaces and concluded that it is stable to the internal kink mode provided the flow speed (the drift speed in MD) increases outwards. B_z is uniform in their equilibrium. The applicability of the MD approximation is rather limited. The inertial effects become important when the flow becomes superfast magnetosonic. This occurs when the flow Lorentz factor exceeds $\Gamma_f \approx \Gamma_{\rm max}^{1/3}$, where $\Gamma_{\rm max}$ is the terminal Lorentz factor corresponding to complete conversion of magnetic energy into the bulk motion energy. Thus MD is justified only for the small initial section of the acceleration zone.

The observations of jets from young stars, X-ray binaries, microquasars, gamma-ray bursts (GRBs) and AGN tell us that their physical parameters differ enormously. One could use this to argue that there exists no single cause for the stability of the various types of jets. However, it would be much more satisfying to have a universal mechanism. In this case, the explanation must be very robust and simple and it must be built around one property common to all these flows. One such common property is the rapid lateral expansion of cosmic jets. With the opening angle of few degrees, the jets of young stellar objects must expand laterally by a factor exceeding 10^4. The radius of the M87 jet near its tip is $r_{\rm j} \sim$ few $\times\ 10^{20}$ cm, indicating the total increase of the jet radius by about 10^6(!) times. Such a dramatic expansion stems from the fact that cosmic jets originate from compact objects, whose gravitational field induces rapid decline of pressure in their surroundings. This is a natural reaction of collimated supersonic flows to the drop of external pressure in their attempt to establish transverse force equilibrium. It has already been pointed out that expansion has a stabilizing effect on jets dynamics (e.g. Rosen & Hardee 2000; Moll, Spruit & Obergaulinger 2008). In our paper, we argue that this is in fact the main reason behind the apparent enhanced stability of cosmic jets.

The issue of stability of cosmic jets is not limited to the problem of their survival. It has been long recognized that emissivity of adiabatically expanding flows drops much faster compared to what is observed in cosmic jets (Begelman, Blandford & Rees 1984) and some 'in situ' dissipation and particle acceleration are required to explain the observations (e.g. Ferrari, Trussoni & Zaninetti 1979; Brunetti et al. 2003; Meisenheimer 2003; Sikora et al. 2005). Internal shocks caused by variability of the central engine and interaction with the environment have been often invoked to introduce such dissipation. However, this may not be sufficient. This is particularly problematic for relativistic shocks in magnetized plasma as the recent particle-in-cell simulations revealed that they are not efficient non-thermal particle accelerators (Sironi & Spitkovsky 2009, 2011). A viable alternative to shocks is the magnetic dissipation associated with magnetic reconnection (e.g. Spruit, Daigne & Drenkhahn 2001; Sironi & Spitkovsky 2014; Sironi, Petropoulou & Giannios 2015). This however requires development of thin current sheets, which may occur naturally via instabilities. Instabilities may also lead to formation of shocks. Such instabilities must be strong and yet not threatening to the jet integrity. These seemingly conflicting requirements can only be met by local internal instabilities, developing on a small scale compared to the jet radius and arising from finer structures inside the jet. In this paper, we give an example of such instability occurring in the magnetically confined jet core.

The observations suggest that global instabilities may also play a role. For example, some cosmic jets appear quite 'wiggly' (e.g. Carilli & Barthel 1996), implying an external kink mode at work. Moreover, the observed properties of Fanaroff–Riley type I (FR-I) extragalactic radio sources indicated that their jets become completely destroyed by instabilities, mix with the external gas and turn

[1] Because of the enormous Reynolds numbers of astrophysical jets, only ideal effects need be considered for the overall stability of the flow.

into buoyant turbulent plumes (e.g. Bicknell 1984). We argue that this loss of jet global stability can occur when it enters regions where the external pressure distribution flattens out. In the case of AGN jets this can be the core of the X-ray corona of the parent galaxy or the extended radio lobe.

This paper is organized in the following way. In Section 2, we put forward very simple and general arguments, which explain how lateral expansion increases global stability of jets. In brief, such expansion slows down, and may even completely terminate, the flow of information across jets, thus reducing the growth of coherent displacements. The rate of expansion depends on the properties of jet surrounding, namely on how fast the external pressure decreases with distance from the jet origin. For power-law atmospheres, $p_{\rm ext} \propto z^{-\kappa}$, there is a critical value for the power index, $\kappa = 2$. For steeper gradients, causal connectivity is lost and the jets are globally stable. In astrophysical context, such steep atmospheres are expected to be quite common. The generality of the argument makes this a very robust and hence attractive explanation, but details depend on the actual internal jet structure. Numerical simulations are required to study the non-linear development of instabilities, particularly in the subcritical regime with $\kappa < 2$. Our efforts in this direction are described in Section 3, where we focus on a particular class of magnetized relativistic jets, whose initial internal structure is described by the core-envelope model of cylindrical jets due to Komissarov (1999). These jets have a z-pinched inner core and a force-free envelope with purely azimuthal magnetic field. A simple method to obtain initial near stationary solutions of relativistic expanding jets was presented in Komissarov, Porth & Lyutikov (2015, hereafter KPL). In Section 3, this approach is generalized in a way which allows us to study the time-dependent 3D dynamics of these flows using periodic box simulations. In both cases, the jet expansion is triggered by a gradual lowering of the external gas pressure, which imitates the conditions experienced by the jet material as it propagates through power-law atmospheres. In Section 5, we discuss the astrophysical implications of our findings. In particular, we propose that the division of extragalactic radio source into FR-I and FR-II classes is related to the stability issue. The lower power FR-I jets are externally confined in the coronas of their host galaxies, which have rather flat pressure distribution, do not expand sufficiently rapidly, become unstable and mix with the coronal plasma on the galactic scale. In contrast, the more powerful FR-II jets remain free and stable until they reach the scales of radio lobes. The instability of jet cores may cause their disintegration and trigger internal dissipation and ultimately electromagnetic emission even when the envelope is stable. This may explain the emission of FR-II jets on much smaller scales than radio lobes. Our conclusions are summarized in Section 6.

2 STABILITY AND CAUSALITY

During the development of instabilities that may threaten the jet integrity, global perturbation modes are amplified. These modes involve coordinated motion of the whole jet and hence imply communication between its different parts by means of waves. These waves trigger forces that push the flow away from its equilibrium state. In the case of unmagnetized fluid, these are sound waves. In magnetized fluids, these are mainly fast magnetosonic waves. If the whole section of the jet is to be displaced to one side of the original jet axis, as this occurs in the kink mode, any part of this section needs to 'know' what the other parts do. In other words, the jet has to be causally connected in the direction transverse to its direction of motion. In the case of supersonic (or superfast magnetosonic) flow, all these waves are advected with the flow and the region of influence of any particular point has the geometry of a cone, aligned with the flow direction. In fluid dynamics, this cone of influence is known as the *Mach cone*. For such flows, the causal communication in the transverse direction is obstructed – no wave can originate at one edge of the cross-section and reach the other. However, a synchronized motion may still be possible as long as an upstream location can be communicated with the whole of the jet somewhere downstream. The higher the Mach number, the longer the separation along the jet between its causally connected sections and slower the growth of unstable perturbation modes become. This is the reason why supersonic flows are less unstable.

For cylindrical jets, this necessary condition for the global instability is always satisfied. This explains why laboratory and terrestrial jets are relatively quickly destroyed by instabilities and why the theoretical studies of flows with cylindrical geometry struggle to explain the stability of cosmic jets. For expanding flows, the situation is more complicated as now there is a competition between the jet expansion and the expansion of the cone of influence. Let us analyse this competition in the simple case of a power-law atmosphere, with pressure $p_{\rm ext} \propto z^{-\kappa}$.

For a start, consider an unmagnetized non-relativistic highly supersonic adiabatic jet. Denote as $\theta_{\rm j} = r_{\rm j}/z$ its half-opening angle and as $\theta_{\rm M}$ its Mach angle. In the limit of small angles, $\theta_{\rm M} = a/v$, where a and v are the sound and bulk motion speeds of the jet, respectively. In such a flow, $v =$const, $\rho \propto r_{\rm j}^{-2}$ and $p \propto \rho^{\gamma}$, which leads to $\theta_{\rm M}/\theta_{\rm j} \propto z\sqrt{p}$. Finally, using $p = p_{\rm ext}$, one finds that

$$\frac{\theta_{\rm M}}{\theta_{\rm j}} \propto z^{(2-\kappa)/2}. \tag{1}$$

Magnetic field introduces an additional degree of complexity as the magnetic hoop stress can result is strong axial pinching of the jet and hence a mismatch between the internal jet pressure and the external one. This is particularly true for magnetically dominated jets, where the magnetic pressure dominates over the thermal one. For scale-free external pressure, one would expect the jets to be self-similar and hence $B^2 \propto p_{\rm ext}$. Away from the central engine the magnetic field is mainly azimuthal and evolves as $B \propto r_{\rm j}^{-1}$, whereas $\rho \propto r_{\rm j}^{-2}$ as before. Thus, the Alfvén speed $c_{\rm a}^2 \propto B^2/\rho \propto r_{\rm j}^0$, the Mach angle based on the Alfvén speed $\theta_{\rm M} \propto r_{\rm j}^0$ and the opening angle $\theta_{\rm j}^{-1} \propto z\sqrt{p_{\rm ext}}$. The last two results ensure that equation (1) still holds in this limit.

The relativistic case is a little bit more complicated as even in the hypersonic regime the thermal energy may dominate the rest-mass energy of gas particles, $p \gg \rho c^2$, and the jet may continue to accelerate. Combining the energy conservation, $p\Gamma^2 r_{\rm j}^2 = $ const, and the mass conservation $\rho\Gamma r_{\rm j}^2 = $ const, where Γ is the jet Lorentz factor and ρ is its comoving density, with the equation of state $p \propto \rho^{\gamma}$, one finds $\Gamma \propto p^{(1-\gamma)/\gamma}$, $r_{\rm j} \propto p^{(\gamma-2)/2\gamma}$, whereas the sound speed is constant, $a = c\sqrt{\gamma - 1}$, and the relativistic Mach angle $\theta_{\rm M} \propto 1/\Gamma$. Taken together, these yield equation (1) again. Thus, equation (1) is quite general.

The form of equation (1) suggests that $\kappa = 2$ is a critical value – for $\kappa < 2$ the jet can remain causally connected, whereas for $\kappa > 2$ the connectivity will be lost. In order to verify this conclusion, we consider a flow characteristic that originates at the jet boundary and moves towards its axis. Its equation is

$$\frac{{\rm d}r}{{\rm d}z} = \theta_{\rm v} - \theta_{\rm M}, \tag{2}$$

where $\theta_{\rm v} = (r/r_{\rm j}){\rm d}r_{\rm j}/{\rm d}z$ is the local streamline angle. Given the lack of characteristic length scale, one may assume that all the jet

parameters are powers of z. In particular, $r_{\rm j} \propto z^{\alpha}$ with $0 < \alpha < 1$ and $\theta_{\rm M} \propto z^{\beta}$. Given these, the solution of equation (2) is

$$r = Az^{\alpha}\left(1 - \frac{C}{\delta}z^{\delta}\right), \tag{3}$$

where A, $C > 0$ are constant and $\delta = 1 + \beta - \alpha$. One can see that the characteristic eventually reaches the jet axis only when $\delta > 0$ – this is a new form of the connectivity condition. In order to turn this condition into the condition of the power index of the atmosphere, we note that

$$\frac{\theta_{\rm M}}{\theta_{\rm j}} \propto z^{\delta}. \tag{4}$$

Comparing this with equation (1), we identify $\delta = (2 - \kappa)/2$ and hence confirm that $\kappa = 2$ is indeed a critical value.

The case of relativistic Poynting-dominated flows is more complicated as the flow is generally not self-similar. In fact, a gradual redistribution of poloidal magnetic flux across the jet is an essential component of the so-called collimation-acceleration mechanism (e.g. Komissarov et al. 2009; Komissarov 2011). However, the analysis presented in Komissarov et al. (2009) shows that $\kappa = 2$ is still a critical value.

When $\kappa > 2$, jets become free, with conical geometry of streamlines. Their pressure decreases rapidly – at least as $z^{-2\gamma}$ in the gas pressure-dominated regime and z^{-4} in the magnetic pressure-dominated one. When this is faster than the external pressure, a reconfinement shock can be driven inside the jet (e.g. Sanders 1983; Komissarov & Falle 1997). Since shock waves are faster compared to sound waves, one may wonder if they can establish pressure balance with the external gas via dissipative heating of jet plasma and support jet connectivity. The key question is whether the reconfinement shock can travel all the way from the jet boundary to its axis. This problem has been analysed in Komissarov & Falle (1997) for the case of unmagnetized uniform relativistic jet and it was found that the shock reaches the axis at the distance

$$z_{\rm r} \simeq \delta^{1/\delta}\left(\frac{L}{a\pi c}\right)^{1/2\delta}, \tag{5}$$

where $\delta = (2 - \kappa)/2$ and a is the coefficient of the law $p_{\rm ext} = az^{-\kappa}$ and L is the jet power. It is easy to see that $z_{\rm r} \to \infty$ as $\kappa \to 2$, which allows us to conclude that for $\kappa > 2$ the jet still remains causally disconnected. Although this analysis is restricted to a particular type of flow, the conclusion must be generic.[2] Indeed, the dynamic pressure of any free jet decreases as $\propto z^{-2}$ and always wins the competition with the external pressure when $\kappa > 2$.

To confirm and illustrate this analysis, we constructed a set of steady-state jet solutions for jet propagating in a power-law atmosphere using the method described in KPL. The jet structure at the nozzle (of radius $r_0 = 1$) is described in Section 3.1. It represents an equilibrium cylindrical flow in pressure balance with the external medium. Fig. 1 shows the results for models with κ ranging between 0.5 and 2.5. First, one can see how the overall jet shape changes from an almost cylindrical for $\kappa = 0.5$ to a conical for $\kappa = 2.5$. Second, these plots nicely illustrate how the jets are trying to maintain the transverse equilibrium by means of magnetosonic waves bouncing across the jet. These waves are launched due to the loss of dynamic equilibrium downstream of the nozzle, where the jet interior becomes underexpanded because of the drop in the external pressure, and cause the oscillations of the jet boundary about the mean position. As κ increases, the wavelength of the oscillations increases as well until they disappear for $\kappa \geq 2$. At this point the causal connectivity across the jet is completely lost.

How does this critical value compare with those of typical environments of cosmic jets? For a polytropic atmosphere of central mass, one has $\kappa = \gamma/(\gamma - 1)$, which is higher than 2 when $1 < \gamma < 2$. For a spherical adiabatic wind, $\kappa = 2\gamma$, which is also steeper than the critical one. (Only a self-collimating magnetic wind can in principle deliver $\kappa < 2$.) For the Bondi accretion $\kappa = 3\gamma/2$, which is still larger than 2 for $\gamma > 4/3$. Thus, steep gradients of external pressure, bordering the critical value, are expected to be quite common close to the central engine.

Observational measurement of gas and magnetic pressure in the environment of cosmic jets is not yet always possible, particularly close to the source. Most of the time, only indirect model-dependent estimates can be made. Taken together, all the estimates available for AGN show that $\kappa \simeq 2$ is a typical mean value for their environment (Phinney 1983; Begelman et al. 1984). To illustrate the arguments, consider the conditions at the jet source. For quasars, we are dealing with $M \simeq 10^9\,{\rm M}_{\odot}$ black holes, which accrete at the rate close to the Eddington's one. The inner parts of their accretion discs are thus dominated by radiation pressure and have constant thickness:

$$H \simeq \frac{3}{2}\left(\frac{\dot{M}c^2}{L_{\rm edd}}\right) r_{\rm g}, \tag{6}$$

where $L_{\rm edd} \simeq 1.3 \times 10^{47}(M/10^9\,{\rm M}_{\odot})\,{\rm erg\ s^{-1}}$ is the Eddington luminosity of mass M and $r_{\rm g} = GM/c^2$ is its gravitational radius (Shakura & Sunyaev 1973). Thus near the black hole, the disc becomes geometrically thick and its vertical hydrostatic equilibrium yields the pressure estimate $p = GM\rho/H$. The gas density can be found from the mass conservation as $\rho = \dot{M}/2\pi r H v_{\rm r}$, where in the α-disc model the accretion speed $v_{\rm r} = \alpha a_{\rm s} H/r$ and $a_{\rm s}^2 \simeq p/\rho$. Combining these equations, we find

$$p = \frac{\dot{M}(GM)^{1/2}}{2\pi\alpha H^{5/2}}. \tag{7}$$

For a $10^9\,{\rm M}_{\odot}$ black hole, this gives us the gas pressure $p_{\rm disc} \simeq (10^7/\alpha)\ {\rm dyn\ cm^{-2}}$ at the scale of order $r_{\rm g} \simeq 1.5 \times 10^{14}$ cm. On the other extreme, inside the extended radio lobes of the size $\simeq 100$ kpc, the typical pressure inferred from the radio and X-ray observations is of the order $p_{\rm lobe} \simeq 10^{-11}\ {\rm dyn\ cm^{-2}}$. Assuming these are the end points of a single power law, we find its index $\kappa \simeq 2$.

Thus, both the theoretical and observational arguments indicate that rapid decline of pressure with distance from their source must be typical for cosmic jets and their corresponding lateral expansion should be fast enough to make a strong positive impact on their global stability. Given the huge range of scales, it would be unrealistic to expect the same slope everywhere. In fact, in hot coronas of elliptical galaxies $\kappa = 1.25 \pm 0.25$ (Mathews & Brighenti 2003). Moreover, inside the extended radio lobes, which expand much slower compared to their sound speed, one would expect $\kappa \simeq 0$. Within such flat sections global instabilities may develop, leading to the observed flaring and wiggling of cosmic jets, whereas through steeper sections they pass mainly undisturbed.

3 PERIODIC BOX SIMULATIONS OF EXPANDING JETS

To study the jet stability, one has to carry out fully three-dimensional simulations, as the most threatening mode is a non-axisymmetric $m = 1$ current-driven mode (Begelman 1998; Appl, Lery & Baty

[2] The dependence of $z_{\rm r}$ on L, a and c can be recovered from the analysis of dimensions. For non-relativistic jets, c has to be replaced with the jet speed.

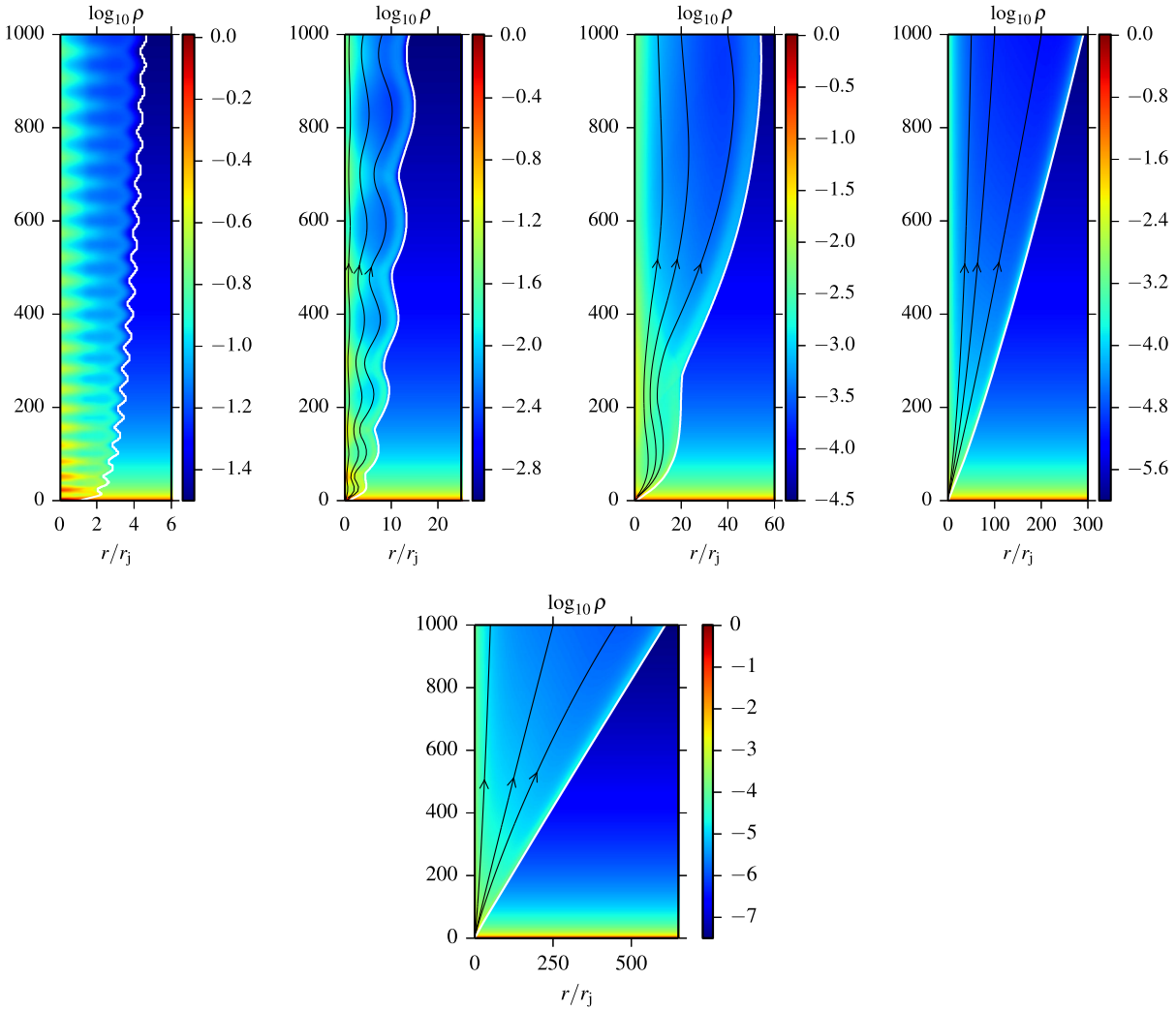

Figure 1. Structure of steady-state jets obtained via time-dependent 1D simulations. The plots show the density distribution for models with $\kappa = 0.5$, 1.0, 1.5, 2.0 and 2.5, increasing from left to right. The distance along the vertical axis is defined as $z = ct/r_j$, where r_j is the initial jet radius. The white contour shows the jet boundary, located using the passive scalar.

2000). For supersonic jets, such instabilities are waves travelling in the general direction of the jet flow and experiencing growth in amplitude downstream. The best way of studying their development is to use very long computational domain, exceeding in size the initial jet radius by several orders of magnitude. Since such simulations are computationally very expensive, much smaller computational domains which capture only a section of the jet have been used in many computational studies instead (for some of the recent examples see Mizuno et al. 2012; Anjiri et al. 2014). To allow travelling waves, such domains are combined with periodic boundary conditions at the boundaries normal to the jet axis. In such a 'periodic box', all waves that leave the computational domain through one of the periodic boundaries, enter it through the opposite one. Obviously, such simulations allow to study only modes whose wavelength is below the box size. To be more precise, a multiple of the wavelength must be equal to the box length. The box frame does not have to be stationary relative to the jet source – it may well be moving relative to it. Clearly, the periodic box simulations are best suited for studying the instability of cylindrical flows ($\kappa = 0$). In order to study the role of the jet expansion in atmospheres with $\kappa > 0$, one may force the external pressure in the box to decrease in a systematic fashion, thus triggering the jet expansion in the radial direction. This is exactly the approach we apply in our simulations.

3.1 Initial conditions

As starting point of our investigation, we choose a cylindrical plasma column in equilibrium between Lorentz forces and pressure gradient. The velocity is directed in vertical direction $v_r = v_\phi = 0$ and the field is purely toroidal. Thus we have the simple relation

$$\frac{\mathrm{d}p}{\mathrm{d}r} + \frac{b^\phi}{r}\frac{\mathrm{d}rb^\phi}{\mathrm{d}r} = 0, \tag{8}$$

where $b^\phi = B^\phi/\Gamma$ is the azimuthal component of the magnetic field as measured in the fluid frame using a normalized basis. One of the infinitely many solutions of equation (8) is the 'core-envelope' model of Komissarov (1999):

$$b^\phi(r) = \begin{cases} b_\mathrm{m}(r/r_\mathrm{m}); & r < r_\mathrm{m}, \\ b_\mathrm{m}(r_\mathrm{m}/r); & r_\mathrm{m} < r < r_\mathrm{j}, \\ 0; & r > r_\mathrm{j}, \end{cases} \tag{9}$$

$$p(r) = \begin{cases} p_0 \left[\alpha + \frac{2}{\beta_m}(1-(r/r_m)^2)\right]; & r < r_m, \\ \alpha p_0; & r_m < r < r_j, \\ p_0; & r > r_j, \end{cases} \quad (10)$$

where

$$\beta_m = \frac{2p_0}{b_m^2}, \qquad \alpha = 1 - (1/\beta_m)(r_m/r_j)^2, \quad (11)$$

r_j is the jet radius and r_m is the radius of its core. As one can see, the core is pinched and in the envelope the magnetic field is force-free. This may be combined with any distribution of density and axial velocity. We imposed $\rho = \rho_0$ and

$$\Gamma(r) = \Gamma_0 \left(1 - (r/r_j)^\nu\right) + (r/r_j)^\nu. \quad (12)$$

The parameters for the initial equilibrium are $r_j = 1$, $r_m = 0.37$, $b_m = 1$, $\rho_0 = 1$, $z_0 = 1$, $\beta_m = 0.34$, $\Gamma_0 = 3$ and $\nu = 2$. The jet is only moderately magnetized with $\sigma_{max} = 0.7$.

We also investigate one force-free jet model where the pressure is set to $p = \alpha p_0$ everywhere in the jet and an additional poloidal field,

$$B^z = \begin{cases} p_0 \left[\frac{2}{\beta_m}(1-(r/r_m)^2)\right]; & r < r_m, \\ 0; & r > r_m, \end{cases} \quad (13)$$

yields the pressure balance in the core. The equation of state used throughout this work is $w = \rho + \gamma/(\gamma-1)p$ with constant adiabatic index $\gamma = 4/3$.

3.2 Numerical treatment

So far periodic box simulations have been used only to study flows with cylindrical geometry, thus excluding the effects of jet expansion. At first glance, this seems to be the only option as the periodic boundary conditions do not allow systematic variation of the external pressure in the jet direction. However, one can use a 'trick' similar to that we have employed in our study of steady jets in KPL – one may trigger the lateral expansion of the jet by forcing the external pressure to decrease. At first, we tried exactly the same approach as in the case of steady jets – direct resetting of the exterior solution to the prescribed state. However, the results of our test experiments with the $\kappa = 0$ model, where we could obtain the solution without forcing and use it as a reference, have shown that this is not quite satisfactory – in the model with forcing the instability turned out to be significantly more violent. The resetting amounts to complete erasing of the instability wave structure outside of the jet. A less drastic approach is to drive the exterior solution towards the desired state according to the relaxation equation

$$\frac{\mathrm{d}f}{\mathrm{d}t} = -\alpha \frac{c}{r_{jet}}(f - f_{ext}(t)), \quad (14)$$

where $f_{ext}(t) = p_0(ct/z_0)^{-\kappa}$ is a target value of the undisturbed state of external gas, f is the actual current value of pressure and $\alpha(c/r_{jet})$ is the relaxation rate. The relaxation rate determines how far the instabilities can penetrate into the jet environment. The method applied in KPL is recovered in the limit $\alpha \to \infty$.[3]

[3] This forcing approach can be applied in the 1D simulations described in KPL. This leads to dampening of jet oscillations but the overall expansion rate is well preserved.

Following Mizuno et al. (2012), we perturb the initial configuration via adding the radial velocity component,

$$v^r(r,\phi,z) = \frac{\Delta v}{N} \exp(-r/r_m) \sum_{n=1}^{N} \cos\phi \sin(2\pi n z/L_z), \quad (15)$$

to the jet velocity field. Here L_z is the box length along the jet axis and N is the number of introduced modes. This corresponds to an equitable superposition of modes with positive and negative azimuthal mode number $m = \pm 1$. In all our simulations we used $N = 4$ and $\Delta v = 0.01\,c$.

In order to select the reasonable relaxation rate constant α, we have carried out test simulations of cylindrical jets ($\kappa = 0$) with and without the forcing term. Fig. 2 shows the snapshots of the solutions for the models which differ only by the value of α, namely $\alpha = 0$, 1/4, 1/2 and 1. One can see that higher value of α leads to more pronounced perturbation of the jet structure. As a reasonable compromise, we adopted $\alpha = 1/2$ for all our main runs.

The simulations have been carried out with MPI-AMRVAC (Keppens et al. 2012; Porth et al. 2014),[4] which utilizes a Godunov-type scheme with Harten–Lax–van Leer (HLL) approximate Riemann solver and second-order spatial total variation diminishing (TVD) reconstruction due to Koren (1993). For the time-advance, we used a three-step Runge–Kutta method. Only on one occasion, near the end of the $\kappa = 2$ run, we had to resort to an even more diffusive Lax–Friedrich scheme to circumvent numerical issues related to extremely low gas pressure in the jet. The solenoidal condition $\nabla \cdot \boldsymbol{B} = 0$ was treated by means of the Dedner et al. (2002) General Linear Modelling (GLM) approach.

In order to determine the required numerical resolution, several models were run with the reference case $\kappa = 0$. A comparison of the results for the average jet magnetization is shown in Fig. 3. Runs with 40 and 80 cells per jet radius agree quite well in both the onset of strong dissipation in the non-linear phase at $t = 40$–50 and in the saturated value obtained at $t \simeq 80$. At 20 cells per jet radius, the solution is markedly more diffused. Based on this data, we have concluded that 20 cells per jet radius is perhaps too low, whereas 80 cells per radius is probably already an 'overkill'. In the expanding simulations, the jet is thus initialized with the resolution of 40 cell per jet radius on the finest adaptive mesh refinement (AMR) grid. The maximum AMR depth was nine levels in the $\kappa = 2$ model while models with $\kappa = 0.5$, 1.0 and 1.5 where run with seven levels. During the runs we refine all cells containing jet material to the current highest level using a passive tracer τ as a jet indicator.

As the jet expands, it becomes better resolved and more and more cells need to be updated. Thus to keep the computational cost at bay, we coarsen the entire jet each time the jet fills more than $N_{max} = 60 \times 10^6$ cells. Assuming the jet retains its approximate cylindrical shape, the number of cells per jet radius just after coarsening the jet to level l is

$$\mathcal{R} = \frac{r_{jet}}{\Delta x} = \frac{1}{2}\left(\frac{N_{max} 2\Delta x}{\pi L_z}\right)^{1/2}, \quad (16)$$

with $\Delta x = 1/40 \times 2^{l_0 - l}$, where l_0 is the AMR level of the jet at the start of the simulations. Hence after the first coarsening event, we have for $L_z = 64$: $\mathcal{R} \simeq 43$, after the second $\mathcal{R} \simeq \sqrt{2} \times 43 \simeq 61$ and so on. Thus the resolution per jet radius effectively increases during the course of the simulation. At the same time, each coarsening event speeds up the simulation by a factor of up to 16 due to the

[4] https://gitlab.com/mpi-amrvac/amrvac

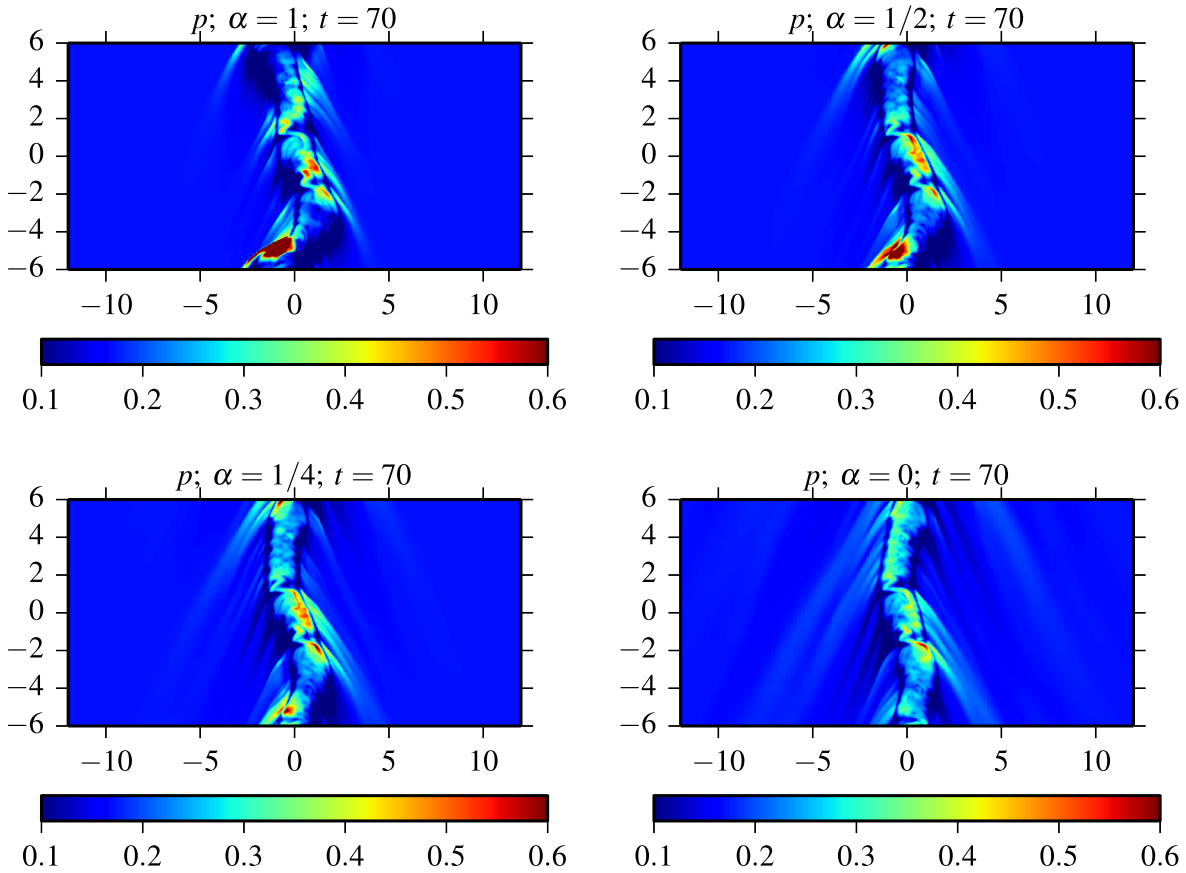

Figure 2. Dependence on the dampening parameter α. The plots show the gas pressure distribution in the $y = 0$ plane for models with $\kappa = 0$ and $\alpha = 1$, 1/2, 1/4 and 0 at the same instance $t = 70$.

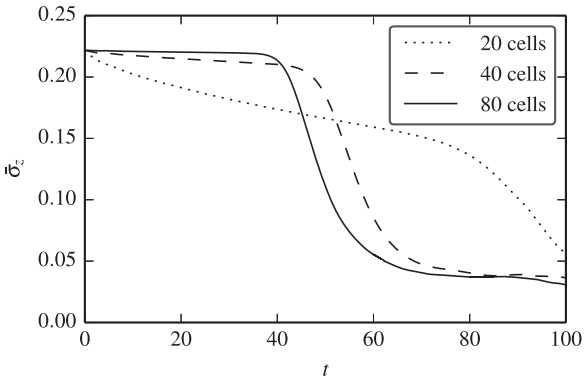

Figure 3. Resolution study of the fiducial parameters with $\kappa = 0$. Resolution is indicated in terms of cells per jet radius $r_j = 1$.

reduced number of cells and the larger Courant–Friedrichs–Lewy (CFL)-limited time step.

The simulations were carried out in a Cartesian domain of the size $(L_x, L_y, L_z) = (192, 192, 64)\, r_j$ for models with $\kappa = 0.5, 1.0$ and 1.5 and $(1536, 1536, 64)\, r_j$ for the model with $\kappa = 2.0$. The jet is centred on the z-axis.

3.3 Results

As expected, models with higher κ turned out to be more stable. Here we first describe our naked eye observations and then provide with quantitative analysis.

In the models with $\kappa = 0.0$ and 0.5, which are relevant for jets surrounded by cocoons (radio lobes in AGN jets), the instability leads to complete disintegration of jets by the end of the simulation runs. Their evolution proceeds in a very similar way but takes 2–3 times longer for the $\kappa = 0.5$ model. The time-evolution of the $\kappa = 0.5$ run is illustrated in Fig. 4. At $t = 100$, where the corresponding non-expanding jet is already disrupted, the $\kappa = 0.5$ model has just entered the non-linear phase. The lateral jet protrusions drive weak compression waves into the ambient medium. The deformations of the jet column become comparable to the jet radius around $t \simeq 200$. At this stage, the compression waves have turned into strong shocks, which begin to transfer a significant amount of the jet power to the environment. By $t = 300$ the jet has lost its integrity and its fragments drive strong bow shocks. By $t = 500$, the effective jet radius has increased to $\approx 50 r_j$, while the size of the corresponding steady-state solution is only $\approx 4 r_j$ at this time. Because of this dramatic increase in the jet cross-section and mixing with the ambient medium, the flow velocity has dropped to a subrelativistic level. The jet has now been totally destroyed and turned into a turbulent plume.

In the model with $\kappa = 1.0$, the value at the lower end for galactic coronas, the jet shows significant fragmentation only by the end of the run, at $t = 1000$. As one can see in Fig. 5, the jet core has fragmented into fast 'bullets' that move through slower and less deformed envelope. The bullet's Lorentz factor is higher compared to the initial one of the core by a factor of 2 – the result of prior thermal acceleration.

In the model with $\kappa = 1.5$, the value on the higher end for galactic coronas, the separation of the core and the envelope becomes even

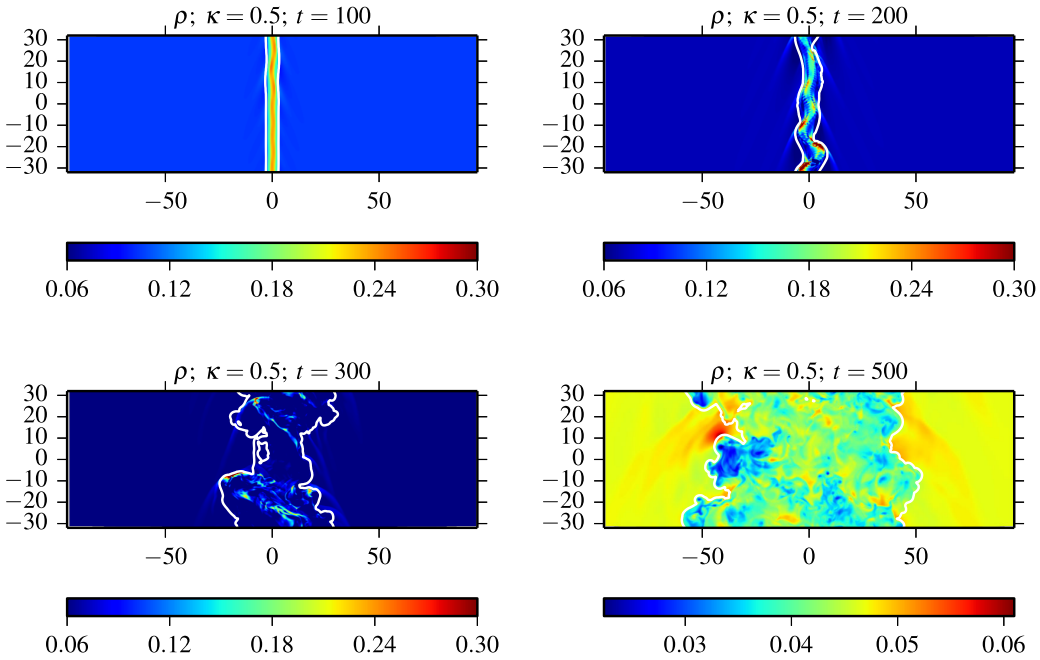

Figure 4. Time evolution of density for the model $\kappa = 0.5$. Shown are $y = 0$ slices for times $t \in \{100, 200, 300, 500\}$. The white contour indicates the jet boundary. The non-linear development of the instability dramatically increases the effective jet cross-section and seeds turbulence in the jet medium ($t = 300$). At $t = 500$ the jet is disrupted entirely and replaced by a slowly moving plume.

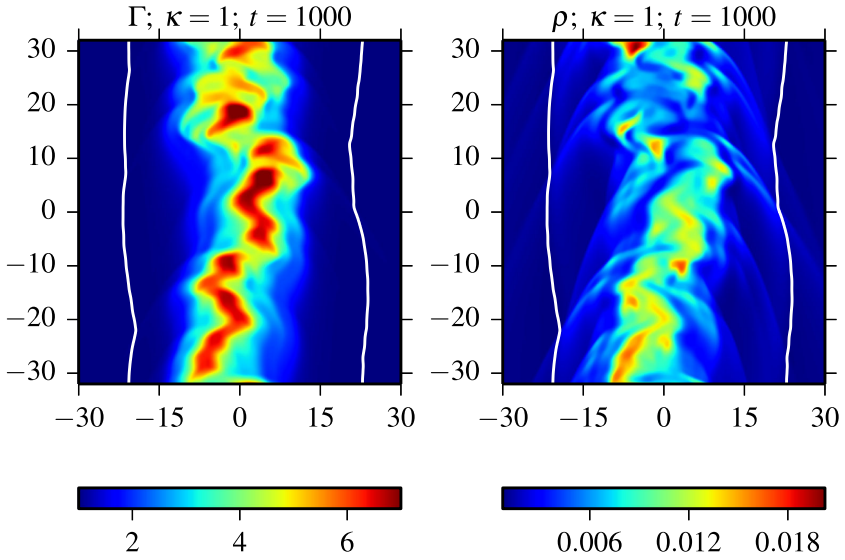

Figure 5. Solution for the model with $\kappa = 1.0$ at $t = 1000$. The white contour indicates the jet boundary.

more prominent (see Fig. 6). By the end of the run ($t = 2000$), the jet radius is approximately the same as in the corresponding steady-state solution and its envelope does not show noticeable deformations. However, already at $t = 1000$ the jet core shows wiggles that have grown out of the initial $n = 4$ mode of the perturbation. These deformations, advected with the fast flow in the core, drive compression waves reminiscent of bow shocks into the jet envelope. One can trace each such wave to a particular wiggle of the core. By $t = 2000$, the initial perturbation starts to fragment the jet core.

Continuing the general trend, at the critical value of $\kappa = 2$ the envelope shows no visible features. The core, however, begins to show noticeable wiggles at $t = 3000$ (see Fig. 7).

The growth of initial perturbations is reflected in the displacement of the jet centre of mass, or barycentre. This displacement is a useful quantitative measure of the amplitude of global instability. We compute the average barycentre displacement in the computational box via integration over the jet cross-section,

$$\bar{r} = \frac{\left| \int Q \boldsymbol{r} \, \mathrm{d}s \right|}{\int Q \, \mathrm{d}s}, \tag{17}$$

and subsequent averaging along the jet axis for the whole box. As a weighting function we choose the relativistic inertia multiplied by the jet tracer

$$Q = \Gamma^2(\rho c^2 + 4p)\tau. \tag{18}$$

Fig. 8 shows the evolution of $\bar{r}$ normalized to the current jet radius $r_{\rm jet}$ for models with different κ. Only in the runs with $\kappa = 0$ and 0.5 jets loose integrity and become fully turbulent by the end of

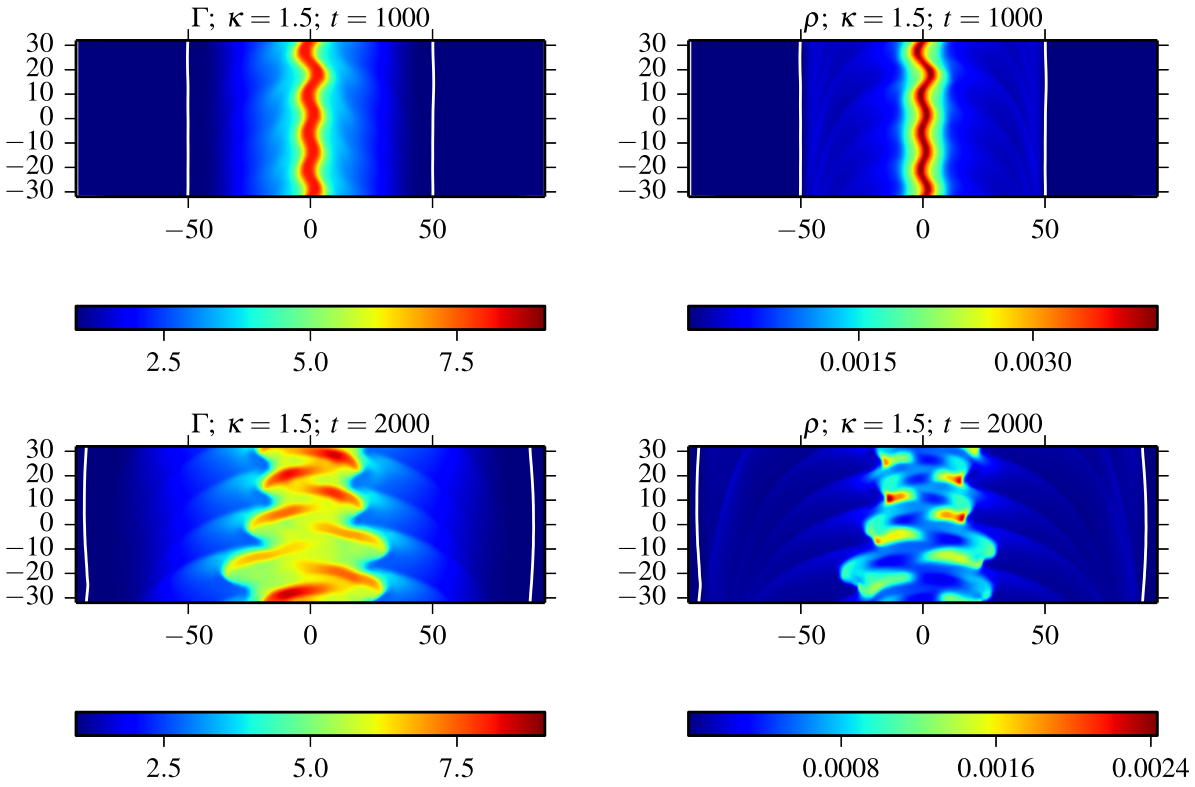

Figure 6. Solution for the model with $\kappa = 1.5$ at $t = 1000$ (top) and at $t = 2000$ (bottom). The white contour indicates the jet boundary.

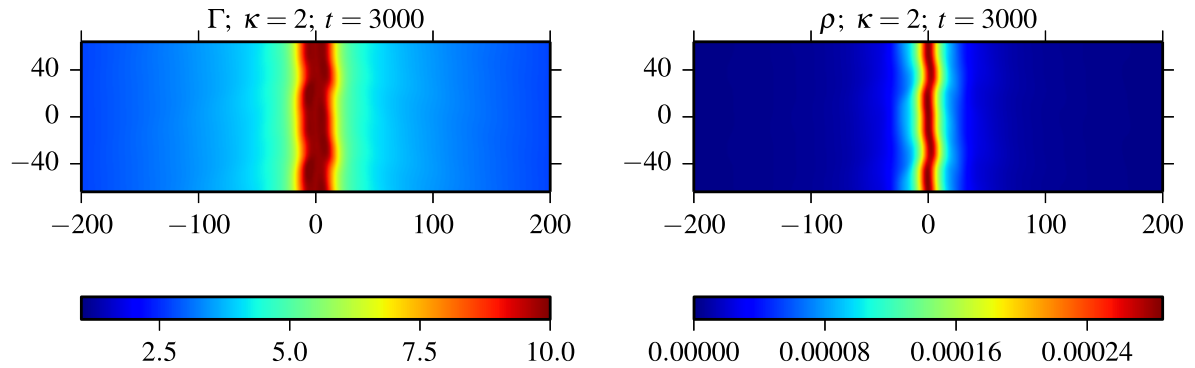

Figure 7. Solution for the model with $\kappa = 2.0$ at $t = 3000$. The jet radius exceeds 200 at this point and its featureless boundary is not seen in these plots.

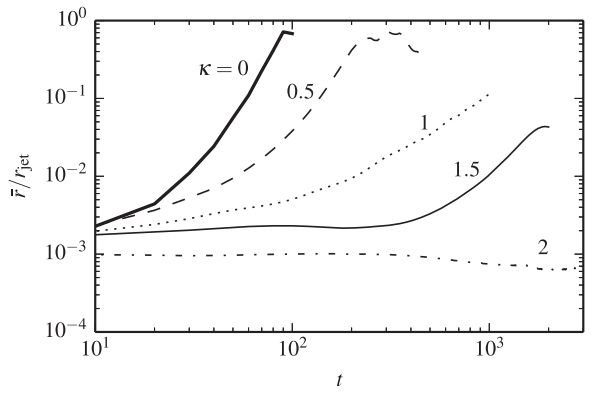

Figure 8. Barycentre displacement normalized to the instantaneous jet radius for increasing values of κ. When $\bar{r}/r_{\rm jet} \gtrsim 0.5$, the jet loses integrity and disrupts.

simulations. Based on these models, we conclude that the disintegration occurs when $\bar{r} = 0.5 r_{\rm jet}$. If the instability does not saturate prior to reaching this amplitude, we expect the jet in the $\kappa = 1$ model to disintegrate around $t =$ few $\times\, 10^3$. In the $\kappa = 1.5$ model, we observe saturation of the core instability at $t \simeq 2000$ and the jet does not loose global integrity due to the modes permitted by the simulation.

Interestingly, for $\kappa = 2$ the normalized barycentre displacement is actually decreasing after $t \simeq 400$, indicating that this jet will never disintegrate, which is fully consistent with our theory. In this run, the jet radius eventually exceeds the length of the computational box, which prompts the question whether this can make a strong impact on the simulation outcome. In order to investigate this issue, we made another run with doubled L_z dimension. For a fair comparison, both cases were perturbed with the same vertical modes. As evidenced in Fig. 9, the resulting dynamics is nearly indistinguishable, showing that the effect of the box size can be neglected.

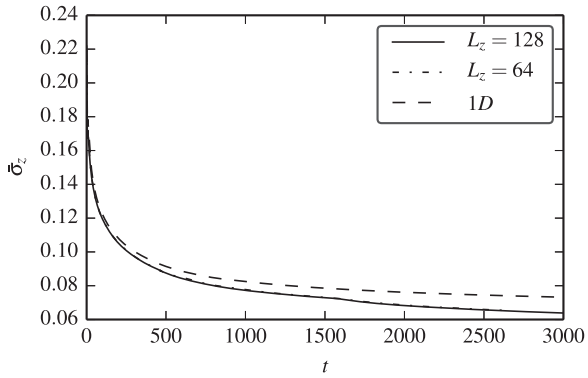

Figure 9. Average jet magnetization in the $\kappa = 2$ models comparing different box sizes with the 1D case.

Fig. 10 compares the energetics of our steady-state and 3D time-dependent solutions for the model with $\kappa = 0.5$. One can see that initially, while the instability amplitude is still small, the jet evolution in both models is more or less the same. This is expected and only proves consistency between these two types of simulations. The dominant process at this phase is the ideal MHD acceleration – as the jet expands, its thermal and magnetic energy is converted into the kinetic energy of bulk motion. In fact, the mean magnetization parameter σ decreases a bit faster in 3D, which is likely to be due to stronger magnetic dissipation.[5] The non-linear effects become important at $t \approx 200$, where the difference between the two solutions becomes quite pronounced. The total of the 3D jet power decreases due to the energy transfer to the external gas via the shock waves driven at first by the jet wiggles and then by its fragments. The instability also generates current sheets inside the jet where the magnetic energy is dissipated. This is further illustrated in Fig. 12, which shows a volume rendering of the current density for two runs with $\kappa = 1$, one with initial helical magnetic field and another with initial toroidal magnetic field. Both solutions exhibit snaking morphology that brings magnetic field lines of different directions closer together. In the model with pure toroidal initial field the current density is noticeably higher.

As a result, the jet's Poynting flux rapidly decreases, and so does its mean magnetization. The dissipated magnetic energy is converted into heat. The process of magnetic dissipation develops rapidly and completes already at $z \approx 400$. After this point the total jet power remains more or less constant – the jet is already very slow and does not drive strong waves into the external medium.

The energetics of the $\kappa = 1$ model is consistent with the early phases of the $\kappa = 0.5$ model (see Fig. 11). In spite of displaying quite pronounced non-axisymmetric distortions and core fragmentation (see Fig. 6), the jet of the $\kappa = 1$ model looses only less than 1 per cent of its total power via emission of MHD waves by the end time of the simulation, at $t = 1000$. For $\kappa = 1.5$ and 2, the difference between the energetics of the steady-state and 3D models is even smaller.

Cores of magnetically generated jets are likely to be dominated not by the gas pressure but by the pressure of poloidal magnetic field. In order to explore the difference this can make on the jet stability, we made another run for the $\kappa = 1.0$ model, now with poloidal magnetic field in the jet core. In this model, the initial radial profiles of the azimuthal component of the magnetic field, density and velocity are the same as before, but the gas pressure

[5] In the simulations we solve equations of ideal relativistic MHD and hence this dissipation is of numerical origin.

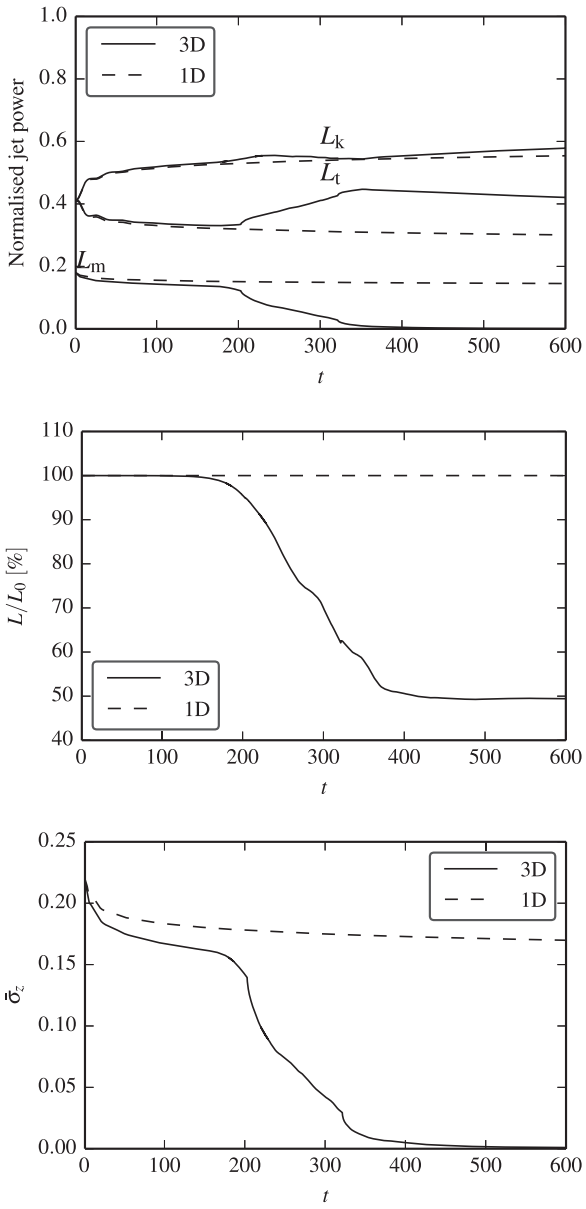

Figure 10. Energetics of jets in the model with $\kappa = 0.5$ – 1D versus 3D. Top: the contributions of kinetic, thermal and magnetic energy to the instantaneous total jet power. Middle: total jet power. Bottom: the volume averaged magnetization parameter σ. Dashed lines show the results for steady-state jets (1D simulations) whereas solid line shows the results of time-dependent 3D simulations.

in the core is uniform and the magnetic field is initially force-free (see KPL for full details). As one can see in Figs 12 and 13, this modification has little effect on the jet stability – in the non-linear regime, the morphology is very similar. However, we note that in the model with initial poloidal field the current density is higher and the current is less fragmented. This can be attributed to the role of the magnetic tension associated with the poloidal field.

4 JET STABILITY AND THE FANAROFF–RILEY DIVISION

The issue of jet stability can be connected to the Fanaroff–Riley (FR) division of extragalactic radio sources into two basic morphological

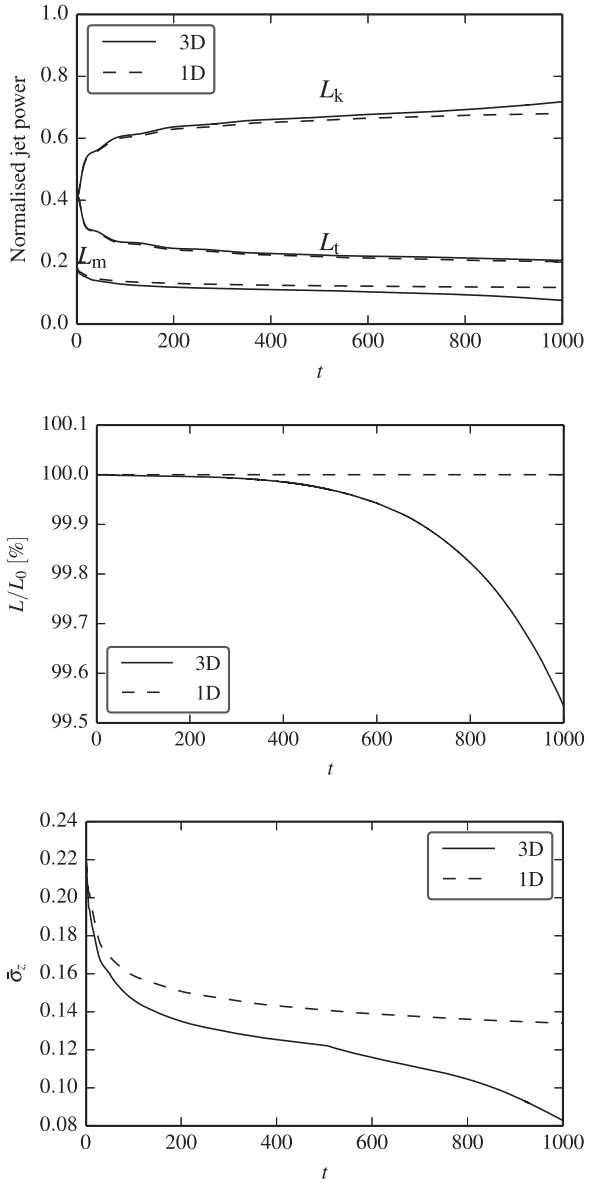

Figure 11. As Fig. 10, but for the model with $\kappa = 1$.

types (Fanaroff & Riley 1974) – FR-I sources with wide two-sided kpc-scale jets and plume-like radio lobes (e.g. 3C 31) and FR-II sources with narrow one-sided jets and cocoon-like radio lobes with leading hotspots (e.g. Cygnus A). In addition to the difference in morphology, these two classes also differ in radio luminosity. The FR-II sources are not just more powerful on average, but there is a sharp division between the two classes on the radio–optical luminosity plane (Owen & Ledlow 1994).

The structure of FR-II radio sources suggests that their jets survive all the way to the leading hotspots, where they collide with the surrounding medium (Blandford & Rees 1974), whereas the structure of FR-I radio sources suggests that their jets suffer destructive global instabilities, become turbulent, entrain dense external gas, slow down to subsonic speeds and turn into plumes (Bicknell 1984; Komissarov 1990a). Observations indicate that on the pc-scale FR-I jets are similar to the FR-II jets – both could be described as well collimated relativistic outflows (Venturi et al. 1995). This indicates that the morphological difference between these types of jets on the kpc-scale is related to the different nature of their interaction with the environment on the length scales around 100 pc.

Given the expected steep decline of the external gas pressure in the galactic nuclei, it is reasonable to assume that soon after leaving the immediate vicinity of the central black hole these jets become free and the global instabilities are suppressed. However, on the scale of about 100 pc they enter the region where the black hole gravity becomes small compared to that of the galaxy. From the X-ray observations, we know that on this scale, the external gas pressure distribution flattens out – here the jets enter the central core region of the galactic X-ray coronas. Further out, on the scale of about 1 kpc, the pressure begins to decline again, though not as steeply as inside AGN. The pressure flattening in the coronal cores creates the necessary condition for the jet reconfinement. This can be important for the jet dynamics, as reconfined jets would become causally connected and hence susceptible to global instabilities. However, the reconfinement process can be too slow to be completed on the core scale. It involves a stationary 'conical' shock wave (the reconfinement shock) gradually converging towards the jet axis. The rate of convergence depends, among other factors, on the jet power. The higher the jet power, the slower this rate becomes. This suggests that more powerful jets may fly through the galactic coronas unimpeded.

The basic geometry of the reconfinement shock can be obtained in the Kompaneets approximation (Kompaneets 1960) which for an unmagnetized relativistic jet leads to

$$\frac{\mathrm{d}r}{\mathrm{d}z} - \frac{r}{z} = -z\left(\frac{p(z)}{K}\right)^{1/2}, \tag{19}$$

where r is the shock radius, $K = \mu L_\mathrm{j}/\pi\theta_0^2 c$, L_j and θ_0 is the power and opening angle of initially free jet, respectively, and μ is a numerical constant of order unity (Komissarov & Falle 1997). In terms of the shock opening angle $\theta = r/z$, dimensionless external pressure distribution $f(z) = p(z)/p_0$ and dimensionless distance $\zeta = z/z_0$, this equation reads

$$\frac{\mathrm{d}\theta}{\mathrm{d}\zeta} = -\theta_0\sqrt{\frac{f(\zeta)}{A}}, \tag{20}$$

where

$$A = \frac{\mu L_\mathrm{j}}{\pi p_0 z_0^2 c} \tag{21}$$

is a dimensionless parameter that combines the effects of the jet power and ambient galactic pressure scale. Integrating equation (20), we find

$$\theta(\zeta) = \theta_0\left(1 - \int_0^\zeta \sqrt{\frac{f(x)}{A}}\mathrm{d}x\right), \tag{22}$$

which gives us the reconfinement scale ζ_r via

$$\int_0^{\zeta_r} \sqrt{f(x)}\mathrm{d}x = \sqrt{A}. \tag{23}$$

Interestingly, ζ_r does not depend on the jet opening angle.

The pressure of galactic coronas is well represented by the model

$$p = p_0\left(1 + (z/z_0)^2\right)^{-\kappa/2}, \tag{24}$$

with $p_0 \simeq 10^{-9}\,\mathrm{dyn\,cm^{-2}}$, $z_0 \simeq 1\,\mathrm{kpc}$ and $\kappa = 1.25 \pm 0.25$ (e.g. Mathews & Brighenti 2003). Using these values we estimate

$$A \simeq \frac{1}{9} p_{0,-9}^{-1} L_{\mathrm{j},44} z_{0,\mathrm{kpc}}^{-2}, \tag{25}$$

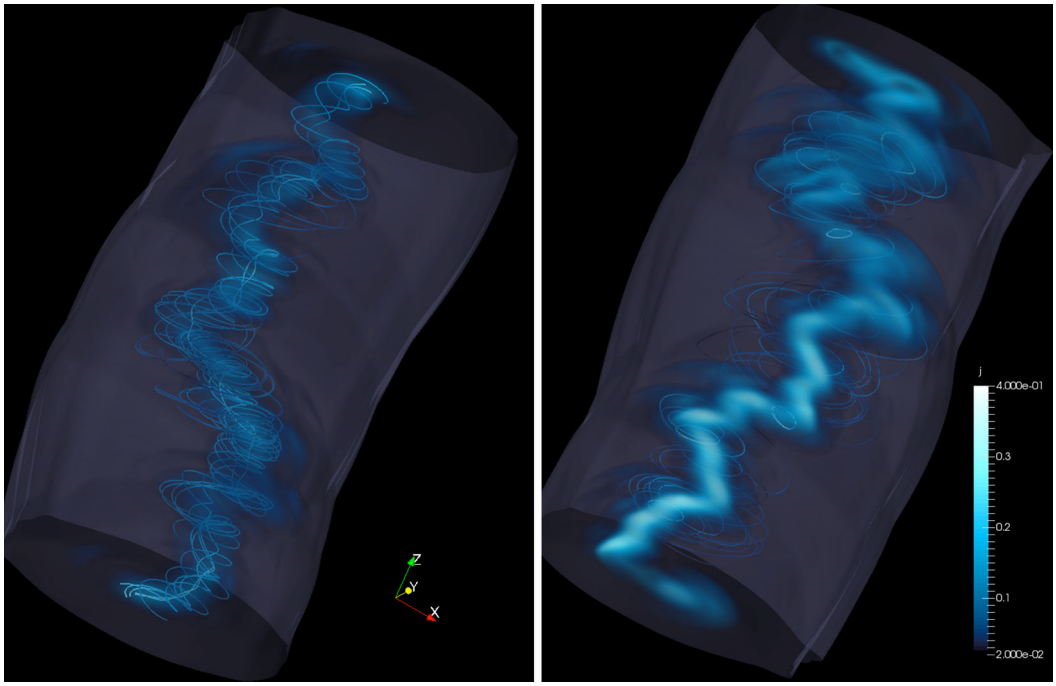

Figure 12. The electric current density and magnetic field structure in models with (left-hand panel) and without (right-hand panel) initial poloidal magnetic field ($\kappa = 1.0$ at $t = 1000$). The outer contour corresponds to the jet boundary.

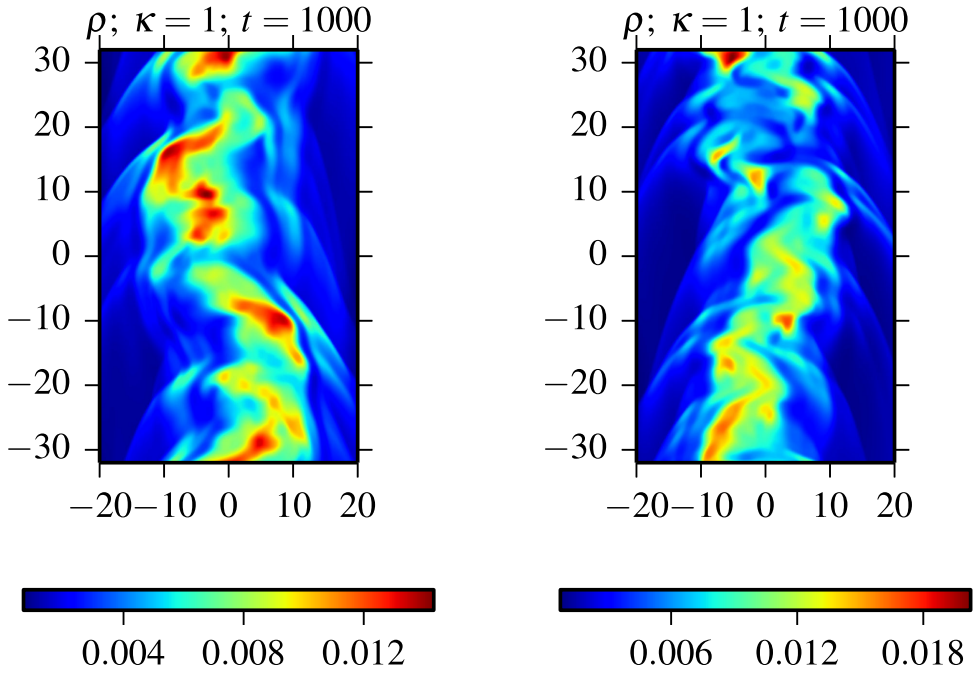

Figure 13. Solutions for models with (left-hand panel) and without (right-hand panel) poloidal magnetic field. The plots show the distribution of rest-mass density for models with $\kappa = 1.0$ at $t = 1000$.

where $p_{0,-9} = p_0/10^{-9}\,\mathrm{dyn\,cm^{-2}}$, $L_{\mathrm{j},44} = L_\mathrm{j}/10^{44}\,\mathrm{erg\,s^{-1}}$ and $z_{0,\mathrm{kpc}} = z_0/1\,\mathrm{kpc}$. Among these parameters, the most scattered one is the jet power and hence it is the jet power which mainly determines how far from the galactic centre the jet becomes reconfined. Based on the energetics of cavities made by the jets in the hot gas of clusters of galaxies, Cavagnolo et al. (2010) give $10^{42} < L_\mathrm{j} < 10^{46}\,\mathrm{erg\,s^{-1}}$, with $L_\mathrm{FR} = 10^{44}\,\mathrm{erg\,s^{-1}}$ separating the FR-I and FR-II classes. Under the assumption that protons can be ignored in the jet energetics, Ghisellini, Tavecchio & Ghirlanda (2009) derived similar top end jet powers via modelling the non-thermal continuum of gamma-ray blazars. If, however, the jet plasma contains equal numbers of protons and electrons, the upper end of the power range extends to $L_\mathrm{j} = 10^{48}\,\mathrm{erg\,s^{-1}}$.

Fig. 14 shows $z_r(L_\mathrm{j})$ for fixed $p_{0,-9} = z_{0,\mathrm{kpc}} = 1$ and $\kappa = 1; 1.5$, the lowest and the highest values of κ which still agree with the observations (Mathews & Brighenti 2003). One can see that for $L_\mathrm{j} \ll L_\mathrm{FR}$ the reconfinement occurs inside the coronal cores ($z_r < z_0$) whereas for $L_\mathrm{j} \gg L_\mathrm{FR}$ well outside of them, at the distances more typical for

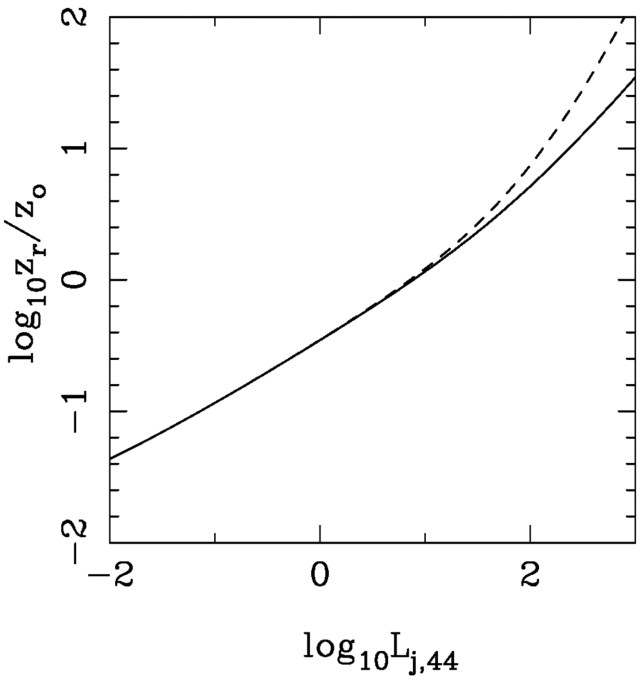

Figure 14. Reconfinement scale in galactic corona as a function of the jet power for $p_{0,-9} = 1$ and $z_{0,\mathrm{kpc}} = 1$. The solutions are shown for $\kappa = 1$ (solid line) and 1.5 (dashed line).

the extended radio lobes. This result provides strong support to the idea that the FR division is rooted in the jet stability. Namely, the jets with power $L_\mathrm{j} < L_\mathrm{FR}$ (FR-I jets) are reconfined inside the galactic coronas, where they become unstable and mix with the coronal plasma, whereas the jets with $L_\mathrm{j} > L_\mathrm{FR}$ (FR-II jets) remain unconfined and hence globally stable on the galactic scale. The FR-II jets may get reconfined further out, inside their radio lobes, where we expect a more-or-less uniform pressure distribution. The kink-mode instabilities in this region may be behind the observed wiggling of the FR-II jets (e.g. Carilli & Barthel 1996) and multiple hotspots (Laing 1981; Scheuer 1982). The non-destructive nature of these instabilities may be down to the fact that the jet mass density is higher than that of lobe density (e.g. Hardee & Rosen 2002).

Another important aspect of the FR division is the dependence of the critical radio luminosity, P_FR, on the optical luminosity of parent galaxies: $P_\mathrm{FR} \propto L_o^2$ (Owen & Ledlow 1994). In our theory of the FR division, this can only be explained via varied parameters of the interstellar gas distribution of parent galaxies (cf. Bicknell 1995). Equation (25) shows that the critical jet power scales as $L_\mathrm{FR} \propto p_0 z_0^2$, so it is important to know how p_0 and z_0 vary with the optical luminosity of the parent galaxy.

The stellar distribution of radio galaxies always shows the presence of a central core (de Ruiter et al. 2005). Kormendy (1987) discovered that the core size increases with optical luminosity as $z_{0,*} \propto L_o^{1.1}$ (see also Faber et al. 1997). The observations also reveal that the optical and X-ray surface brightness profiles of elliptical galaxies are almost identical (Trinchieri, Fabbiano & Canizares 1986), which suggests that the size of the X-ray core $z_0 \propto L_o^{1.1}$ as well. The X-ray luminosity of the elliptical galaxies is approximately $L_x \propto L_o^2$ (O'Sullivan, Forbes & Ponman 2001). Ignoring the weak dependence of the X-ray emissivity on the temperature, we have $L_x \propto n_0^2 z_0^3$, which yields $n_0 \propto L_o^{-1/2}$. Assuming that the temperature itself arises from collisions of gas clouds ejected by stars, it depends on the stellar velocity dispersion as $T \propto \sigma^2$. The same result follows when the X-ray gas is modelled as an isothermal hydrostatic sphere (Bicknell 1995). Given the Faber–Jackson relationship $\sigma \propto L_o^{0.25}$ (Faber & Jackson 1976; Terlevich et al. 1981), which is a convenient projection of the less scattered Fundamental Plane (Djorgovski & Davis 1987; Dressler et al. 1987), this reads as $T \propto L_o^{1/2}$ and hence $p_0 \propto n_0 T \propto L_o^0$ is independent of the optical luminosity. Thus we find that the critical jet power

$$L_\mathrm{FR} \propto p_0 z_0^2 \propto L_0^{2.2}, \tag{26}$$

which agrees very well with the observational results by Owen & Ledlow (1994).

The Kompaneets approximation, which assumes constant pressure across the shocked layer, may lead to a substantial error for the reconfinement distance. For example, the calculations of Nalewajko & Sikora (2009), which account for the pressure variation in the shocked layer, show a factor of 2 difference in the case of uniform external medium. Moreover, equation (20) ignores the role of magnetic field. Future studies will clarify these issues.

5 DISCUSSION

The results of our numerical simulations confirm the strong dependence of instabilities on the jet expansion associated with decline of external pressure. Although we considered only one particular case of transverse jet structure out of infinitely many possible configurations of various types, the underlying reason is very generic – full or partial loss of causal connectivity – and should operate for all types of supersonic jets, relativistic or not.

In studies of cylindrical static columns, it has been found that our test configuration is disruptively unstable to kink mode instabilities, in contrast to configurations with force-free magnetic field, which are found to be much more stable and exhibit only mild coherent deformations at the non-linear phase (O'Neill et al. 2012).[6] Does this mean that such force-free configurations, where the magnetic force associated with the azimuthal component is finely balanced by the forces associated with the poloidal component, are vastly superior and can provide an alternative explanation to the stability of cosmic jets? Likely not. Indeed, as this has already been pointed out by O'Neill et al. (2012), strong expansion of cosmic jets is bound to destroy such force-free equilibrium because in expanding jets the poloidal field decays faster than the azimuthal one. In magnetically dominated equilibrium jets this should lead to $b^\phi \propto r^{-1}$, which is exactly what we postulated for the envelope of our initial solutions. Our runs with and without the poloidal component already support this conclusion and future studies will clarify this issue further.

On the one hand, mild global deformations are preferable because they preserve jet integrity. On the other hand, they are also deficient, being unable to trigger dissipation, particle acceleration and ultimately non-thermal emission of cosmic jets. The solution to this conundrum could be found in local instabilities, which do not endanger the global integrity of jets. In this regard, the core-envelope structure of magnetized jets is a very attractive feature. Indeed, disintegration of the core via kink instability does not have to be fatal for the whole jet when the jet is much wider.

A slowly expanding core seems to be a generic property of jets with dynamically important helical magnetic field. For

[6] In fact, they considered a somewhat different distribution of the azimuthal magnetic field in the envelope, with b^ϕ decreasing more like r^{-2} than r^{-1}. Nonetheless, we have seen that our cylindrical configuration was similarly unstable and hence this deviation is not significant.

magnetically accelerated jets from rotating bodies this is well known (e.g. Bogovalov 1995; Beskin & Nokhrina 2009). In our models, there is no rotation and the slow expansion of the jet core is of a somewhat different nature. It arises from properties of the z-pinch equilibrium, where the hoop stress of the azimuthal component of magnetic field balances the pressure force. In order to elucidate this point, consider the non-relativistic case, which is much simpler. For magnetically dominated envelope with predominantly azimuthal magnetic field, its force equilibrium requires $B_\phi = B_{\rm m}(r/r_{\rm m})^{-1}$, in which case the hoop stress is balanced by the pressure force of the azimuthal field itself. However, this profile cannot be extended all the way to the jet axis, as this would lead to infinite magnetic energy. Instead it terminates at the core radius $r_{\rm m}$. In order to avoid infinite current density, B_ϕ should actually vanish at $r = 0$. The conservation of magnetic flux of the envelope then requires

$$B_{\rm m} \propto (r_{\rm m} \log(r_{\rm jet}/r_{\rm m}))^{-1}. \quad (27)$$

Inside the core, the hoop stress should be balanced either by the gas pressure or the pressure of the poloidal magnetic field. If the total core pressure is dominated by the gas contribution, then it evolves as $p_{\rm c} \propto r_{\rm m}^{-2\gamma}$. The transverse force balance of the jet core can be approximated as $p_{\rm c}/r_{\rm m} \propto B_{\rm m}^2/r_{\rm m}$, which yields

$$r_{\rm m} \propto (\log(r_{\rm jet}/r_{\rm m}))^{1/(\gamma-1)}. \quad (28)$$

If it is the pressure of the poloidal magnetic field which dominates in the core, then equation (28) still applies if we put $\gamma = 2$. One can see that in both these cases the core radius grows much slower than the jet radius. To put this in a different way, if the core radius expanded as fast as the jet radius, then the hoop stress would decrease as $r_{\rm jet}^{-3}$ whereas the core pressure force would drop faster, in conflict with the assumed force equilibrium.

A fraction of the dissipated magnetic energy of the core can be emitted and the rest converted into the kinetic energy (cf. Giannios & Spruit 2006). The result could be a fast and luminous spine surrounded by slow and relatively dark sheath. In the sheath, the magnetic field would be mainly azimuthal, whereas in the spine its structure would be determined by the competition between the turbulent randomization, stretching by mean velocity field and shock compression. Such 'spine–sheath' structure can explain many observations of AGN jets (e.g. Komissarov 1990b; Bridle 1996; Stawarz & Ostrowski 2002; Giroletti et al. 2004; Ghisellini, Tavecchio & Chiaberge 2005; Gopal-Krishna et al. 2007; Laing & Bridle 2014). Fragmentation of the jet core can also explain why the superluminal blobs of AGN jets occupy only a portion of the entire jet cross-section (Lister 2013). The envelope, with its largely undisturbed azimuthal field, can be behind the transverse gradients of the Faraday rotation measure found in many parsec-scale AGN jets (Gabuzda 2013). If the whole jet was affected by the kink instability and developed turbulence, one would not expect to find regular azimuthal field and hence the Faraday rotation gradients on the scale of jet radius.

Very long baseline interferometry (VLBI) observations of AGN jets allow to measure the Lorentz factor of their moving blobs $\Gamma_{\rm b}$ and the jet half-opening angle $\theta_{\rm j}$. These measurements lead to the result $\Gamma_{\rm b}\theta_{\rm j} \approx 0.2$ (Jorstad et al. 2005; Clausen-Brown et al. 2013), which seem to indicate that these jets are causally connected and therefore externally confined. This conclusion is supported by the observed acceleration of the blobs in blazar jets up to the deprojected distance of $\simeq 100$ pc (Homan et al. 2015), which turns into a deceleration at larger distances. Indeed, this can been interpreted as an evidence of the magnetic collimation acceleration mechanism (Vlahakis & Königl 2004; Komissarov et al. 2007, 2009; Lyubarsky 2010), which requires external confinement. In fact, the observations of the M87 jet are not only in agreement with the MOJAVE data on the continued acceleration up to the distance of $\simeq 100$ pc, where the stationary HST-1 feature is located, but also indicate the parabolic shape of the jet, $z \propto r^{1.7}$, in this region (Asada & Nakamura 2012; Asada et al. 2014). Further out the jet becomes conical and its speed decreases. These data challenge the key point of our theory that on the scales below 100 pc the AGN jets are unconfined.

However, a closer look at the observational data shows a number of problems with this interpretation. For $p \propto z^{-\kappa}$ with $\kappa < 2$ the collimation acceleration theory predicts the jet shape $z \propto r^a$, where the index $a = 4/\kappa > 2$ (Komissarov et al. 2009; Lyubarsky 2009), in conflict with the observations of M87 which give $a < 2$. Asada & Nakamura (2012) applied the theoretical results for the degenerate case $\kappa = 2$, which allows $1 < a < 2$ depending on the initial jet structure. However, because these transitional cases require κ to be exactly 2, it is hard to see how they can be of more than just mathematical interest. For $\kappa > 2$ the flows are asymptotically conical.

Moreover, for $\kappa < 2$ the theory predicts $\Gamma_{\rm j} \simeq r/r_{\rm lc}$, where $r_{\rm lc}$ is the radius of the light cylinder. For a Blandford–Znajek jet from a rapidly rotating black hole, $r_{\rm lc} \approx 2r_{\rm s}$, where $r_{\rm s} = 2GM/c^2$ is the Schwarzschild radius. Thus, one would expect the typical Lorentz factor of blazar jets $\Gamma \approx 10$ to be reached when the jet radius just exceeds $r_{\rm j} = 20r_{\rm s}$. In contrast, for the typical half-opening angle of blazar jets, $\theta_{\rm j} = 0.02$, the jet radius at the distance of 100 pc is much larger: $r_{\rm j} \approx 6 \times 10^{18}$ cm $\approx 2 \times 10^4 r_{\rm s}$ for a $10^9\,{\rm M}_\odot$ black hole. Thus, the asymptotic value of the Lorentz factor $\Gamma_{\rm max} \approx 10$ would have been reached on much smaller scales than observed. These estimates may not be very accurate for flows with only moderate asymptotic Lorentz factor, but the results of numerical simulations of such flows confirm that the acceleration of AGN jets should be almost fully completed inside the first parsec (Komissarov et al. 2007).

For a slowly rotating black hole $r_{\rm ls} \approx (4/a)r_{\rm s}$, where a is the rotation parameter, so $\Gamma_{\rm j} = 10$ would be reached when $r_{\rm j} = (40/a)r_{\rm s}$. This can be matched with the observed jet radius at the end of the acceleration zone only for the incredibly low $a = 0.002$. If the jet originates from a Keplerian disc, then $r_{\rm lc} = \sqrt{2}r_{\rm s}(r_{\rm f}/r_{\rm s})^{3/2}$, where $r_{\rm f}$ is the radius of the magnetic foot-point on the disc. To match the observations, we would need $r_{\rm f} \approx 140r_{\rm s}$, which is too far from the disc inner edge. In both these cases, it will be very difficult to explain the high power of blazar jets.

It could be that the VLBI observations do not reveal the entire structure of AGN jets, but only their bright magnetically confined inner cores. Their enhanced brightness is a combination of magnetic pinch and dissipation triggered by kink-mode instabilities. The magnetic dissipation may also power the observed bulk acceleration. It has been known for some time that at the kpc scale even the minimal pressure of the M87 jet is about one order of magnitude above the external gas pressure, which can be interpreted as an evidence of magnetic confinement (Biretta, Owen & Hardee 1983; Owen, Hardee & Cornwell 1989). However, the polarization observations show that the magnetic field is predominantly aligned with the jet (Owen, Hardee & Bignell 1980; Owen et al. 1989). This is qualitatively consistent with the M87 jet being only the jet core, where the magnetic field structure is randomized by instabilities and stretched by velocity shear. It is well known that the poloidal field in kpc-jets cannot be regular as this leads to enormous magnetic flux, which cannot be sustained by any reasonable central engine (Begelman et al. 1984). Where is the azimuthal magnetic field responsible for the magnetic confinement? Perhaps, it is in the

free-expanding jet envelope which is dim because it is stable and the dissipation is not triggered in it and because it is slow and its emission is not Doppler beamed. The Faraday rotation gradients across jets may have already revealed its presence (Algaba, Asada & Nakamura 2013; Gabuzda 2013).

Falle & Wilson (1985) explained the apparent overpressuring of the M87 jet by the compression at standing conical shocks. However, the pressure jumps in their model are smaller than the observed ones, even if the minimal pressure represents the total jet pressure, and the structure of M87 knots does not have sharp features easily associated with conical shock geometry (Biretta et al. 1983; Owen et al. 1989).

In this paper, focused primarily on AGN jets, which is a reflection of the authors' main research area. However, the strong lateral expansion is a common property of all astrophysical jets and in this regard our results must have much broader application. Since these jets originate from central objects whose gravity dictates the properties of their environment, strong stratification with steep pressure gradients, promoting free expansion of jets, must be very common. Jets from young stars, X-ray binaries and collapsing stars are likely to be surrounded by broad winds originating in the same central objects. For a spherical adiabatic wind, the wind gas pressure drops as $p \propto z^{-\kappa}$ with $\kappa = 2\gamma > 2$. Adiabatic spherical accretion on a point-like central mass gives $\kappa = 3\gamma/2$ (Bondi 1952). In collapsing stellar envelopes, the gas pressure follows a similar law, whereas for the ram pressure $\kappa = 5/2$ (Bethe 1990). In all these cases the pressure gradient is sufficiently steep to promote free expansion of jets and suppress instabilities via the loss of causal connectivity. From the observations of 'jet-breaks' in the emission of GRB afterglows one can estimate the product of the jet opening angle and its Lorentz factor, $10 < \Gamma_j\theta_j < 50$ (Panaitescu & Kumar 2002). For kinetic-energy-dominated flows this actually implies a total loss of causal connectivity (e.g. Zakamska, Begelman & Blandford 2008). However, for Poynting-dominated flows the condition $\Gamma_j\theta_j > 1$ is not sufficient to infer a causally disconnected flow as the fast magnetosonic sound speed can be much closer to the speed of light (Komissarov et al. 2009).

The periodic box approach has its obvious limitations – it does not allow us to study wavelengths exceeding the box size and does not fully reproduce the conditions in expanding jets. In future, larger boxes may have to be utilized for systematic studies of flows with strong poloidal magnetic field, which may suppress the growth of short-wavelength perturbations. Another option is to resort to computationally expensive simulations in large non-periodic boxes. In this case, on can include the magnetorotational central engine as a part of the problem and ensure that the jet structure is consistent with its origin, which is an indisputable advantage (see e.g. Moll et al. 2008; McKinney & Blandford 2009; Porth 2013). Interestingly, the stable jet simulated in McKinney & Blandford (2009) has an almost conical geometry, which is a characteristic of free expansion in steep 'atmosphere'. In these simulations the jet engine is initially surrounded by an almost empty space but later the inner region if filled with the disc wind. Overall, the pressure decreases with distance faster than z^{-2} (McKinney, private communication), consistent with the conclusions of our work.

In this paper, we focused on relatively simple atmospheres described by power-law and King-type distributions. The reality is likely to be more complicated. For example, AGN jets may cross quasi-standing shocks resulting from the interaction between a wide disc wind and interstellar medium (ISM). This would put the jet strongly off the lateral force balance with ISM after the crossing and drive in a reconfinement shock. In such strongly off-balance cases the reconfinement shock may actually reach the jet centre even when $\kappa > 2$ (Bromberg & Levinson 2007; Kohler, Begelman & Beckwith 2012). A non-relativistic magnetized disc wind may also play an important role in collimating the jets (Gracia, Tsinganos & Bogovalov 2005). We plan to explore these avenues in future studies.

6 CONCLUSIONS

Typical environmental conditions of cosmic jets include rapid decline of pressure with distance from the jet source. Our analysis shows that for atmospheres with the power law $p_{\rm ext} \propto z^{-\kappa}$ pressure distribution, the value $\kappa = 2$ is critical in the sense that a steeper pressure decline leads to such a rapid lateral jet expansion that the causal communication across the jet is completely lost and hence global instabilities of any type become totally suppressed. We propose that this is the reason for the observed remarkable stability of jets from young stars and AGN, which are capable of propagating distances which exceed their initial radius up to a billion times.

Our numerical simulations are in full agreement with this conclusion. They convincingly demonstrate the reduction of the growth rate of the kink instability with increase of the power index κ, and suggest global jet stability for $\kappa \geq 2$. In the simulations, we considered only one particular type of jets, but in combination with the very general analytical arguments they make a strong case in favour of the proposed explanation of the apparent stability of cosmic jets.

When cosmic jets enter flat sections of external atmospheres, they may reconfine and re-establish causal connectivity. This creates conditions for global instability. We have analysed the reconfinement process of extragalactic jets in the X-ray coronas of their parent galaxies, which have relatively flat pressure distribution, and found that, depending on the jet power, the reconfinement may occur both deeply inside the coronal core and well outside of it, on scales more characteristic of radio lobes. The separation between the two cases roughly corresponds to the jet power at the border line between FR-I and FR-II radio sources. This suggests that the FR-I jets get reconfined, become unstable and form turbulent plumes on the scale of the coronal core, whereas the FR-II jets burst through the corona largely unscathed. The critical jet power depends on the pressure and radius of the X-ray core. Using the empirical properties of elliptical galaxies, we derived the relationship between critical power and the optical luminosity of the host galaxy, which in a very good agreement with the observations.

Jets with dynamically important magnetic field tend to be highly non-uniform, owing to the hoop stress of the azimuthal component of the magnetic field. When a jet develops a z-pinched core, this core expands much slower than the jet envelope and can preserve causal connectivity across itself. As the result, it becomes susceptible to instabilities. In our simulations we observed non-linear development of such instabilities, which resulted in core fragmentation and its energy dissipation. Such local instabilities do not present a threat to the integrity of the whole jet but they may be responsible for its observed emission and morphology. The so-called 'spine–sheath' structure of AGN, supported by various observations, is one likely outcome.

ACKNOWLEDGEMENTS

SSK and OP are supported by STFC under the standard grant ST/I001816/1. The computations were carried out on the UK MHD cluster Arc-I in Leeds and Dirac-II in Durham. OP likes to thank Purdue University for kind hospitality.

REFERENCES

Algaba J. C., Asada K., Nakamura M., 2013, European Phys. J. Web Conf., 61, 7003
Anjiri M., Mignone A., Bodo G., Rossi P., 2014, MNRAS, 442, 2228
Appl S., Lery T., Baty H., 2000, A&A, 355, 818
Asada K., Nakamura M., 2012, ApJ, 745, L28
Asada K., Nakamura M., Doi A., Nagai H., Inoue M., 2014, ApJ, 781, L2
Bateman G., 1978, MHD Instabilities. MIT Press, Cambridge, MA
Baty H., Keppens R., 2002, ApJ, 580, 800
Begelman M. C., 1998, ApJ, 493, 291
Begelman M. C., Blandford R. D., Rees M. J., 1984, Rev. Modern Phys., 56, 255
Beskin V. S., Nokhrina E. E., 2009, MNRAS, 397, 1486
Bethe H. A., 1990, Rev. Modern Phys., 62, 801
Bicknell G. V., 1984, ApJ, 286, 68
Bicknell G. V., 1995, ApJS, 101, 29
Biretta J. A., Owen F. N., Hardee P. E., 1983, ApJ, 274, L27
Birkinshaw M., 1991, in Hughes P. A., ed., Beams and Jets in Astrophysics. Cambridge Univ. Press, Cambridge, p. 278
Blandford R. D., Rees M. J., 1974, MNRAS, 169, 395
Blandford R. D., Znajek R. L., 1977, MNRAS, 179, 433
Bogovalov S. V., 1995, Astron. Lett., 21, 565
Bondi H., 1952, MNRAS, 112, 195
Bridle A. H., 1996, in Hardee P. E., Bridle A. H., Zensus J. A., eds, ASP Conf. Ser. Vol. 100, Energy Transport in Radio Galaxies and Quasars. Astron. Soc. Pac., San Francisco, p. 383
Bromberg O., Levinson A., 2007, ApJ, 671, 678
Brunetti G., Mack K.-H., Prieto M. A., Varano S., 2003, MNRAS, 345, L40
Carilli C. L., Barthel P. D., 1996, A&AR, 7, 1
Cavagnolo K. W., McNamara B. R., Nulsen P. E. J., Carilli C. L., Jones C., Bîrzan L., 2010, ApJ, 720, 1066
Clausen-Brown E., Savolainen T., Pushkarev A. B., Kovalev Y. Y., Zensus J. A., 2013, A&A, 558, A144
Dedner A., Kemm F., Kröner D., Munz C.-D., Schnitzer T., Wesenberg M., 2002, J. Chem. Phys., 175, 645
de Ruiter H. R., Parma P., Capetti A., Fanti R., Morganti R., Santantonio L., 2005, A&A, 439, 487
Djorgovski S., Davis M., 1987, ApJ, 313, 59
Dressler A., Lynden-Bell D., Burstein D., Davies R. L., Faber S. M., Terlevich R., Wegner G., 1987, ApJ, 313, 42
Faber S. M., Jackson R. E., 1976, ApJ, 204, 668
Faber S. M. et al., 1997, AJ, 114, 1771
Falle S. A. E. G., Wilson M. J., 1985, MNRAS, 216, 79
Fanaroff B. L., Riley J. M., 1974, MNRAS, 167, 31p
Ferrari A., Trussoni E., Zaninetti L., 1979, A&A, 79, 190
Freidberg J. P., 1982, Rev. Modern Phys., 54, 801
Gabuzda D. C., 2013, European Phys. J. Web Conf., 61, 7001
Ghisellini G., Tavecchio F., Chiaberge M., 2005, A&A, 432, 401
Ghisellini G., Tavecchio F., Ghirlanda G., 2009, MNRAS, 399, 2041
Giannios D., Spruit H. C., 2006, A&A, 450, 887
Giroletti M. et al., 2004, ApJ, 600, 127
Gopal-Krishna, Dhurde S., Sircar P., Wiita P. J., 2007, MNRAS, 377, 446
Gracia J., Tsinganos K., Bogovalov S. V., 2005, A&A, 442, L7
Hardee P. E., 2011, in Romero G. E., Sunyaev R. A., Belloni T., eds, Proc. IAU Symp. 275, Jets at All Scales. Cambridge Univ. Press, Cambridge, p. 41
Hardee P. E., Hughes P. A., 2003, ApJ, 583, 116
Hardee P. E., Rosen A., 2002, ApJ, 576, 204
Homan D. C., Lister M. L., Kovalev Y. Y., Pushkarev A. B., Savolainen T., Kellermann K. I., Richards J. L., Ros E., 2015, ApJ, 798, 134
Istomin Y. N., Pariev V. I., 1994, MNRAS, 267, 629
Jorstad S. G. et al., 2005, AJ, 130, 1418
Keppens R., Meliani Z., van Marle A., Delmont P., Vlasis A., van der Holst B., 2012, J. Chem. Phys., 231, 718
Kohler S., Begelman M. C., Beckwith K., 2012, MNRAS, 422, 2282
Komissarov S. S., 1990a, Ap&SS, 171, 105
Komissarov S. S., 1990b, Soviet Astron. Lett., 16, 284
Komissarov S. S., 1999, MNRAS, 308, 1069
Komissarov S. S., 2002, MNRAS, 336, 759
Komissarov S. S., 2011, Mem. Soc. Astron. Ital., 82, 95
Komissarov S. S., Falle S. A. E. G., 1997, MNRAS, 288, 833
Komissarov S. S., Barkov M. V., Vlahakis N., Königl A., 2007, MNRAS, 380, 51
Komissarov S. S., Vlahakis N., Königl A., Barkov M. V., 2009, MNRAS, 394, 1182
Komissarov S. S., Porth O., Lyutikov M., 2015, Comput. Astrophys. Cosmol., preprint (arXiv:1504.07534) (KPL)
Kompaneets A. S., 1960, Soviet Phys. Doklady, 5, 46
Koren B., 1993, in Vreugdenhil C. B., Koren B., eds, Notes on Numerical Fluid Mechanics, Vol. 45, Numerical Methods for Advection–Diffusion Problems. Vieweg, Braunschweig, p. 117
Kormendy J., 1987, in de Zeeuw P. T., ed., Proc. IAU Symp. 127, Structure and Dynamics of Elliptical Galaxies. Reidel, Dordrecht, p. 17
Laing R. A., 1981, MNRAS, 195, 261
Laing R. A., Bridle A. H., 2014, MNRAS, 437, 3405
Lister M. L., 2013, European Phys. J. Web Conf., 61, 6002
Lyubarskii Y. E., 1999, MNRAS, 308, 1006
Lyubarsky Y., 2009, ApJ, 698, 1570
Lyubarsky Y. E., 2010, MNRAS, 402, 353
McKinney J. C., Blandford R. D., 2009, MNRAS, 394, L126
Mathews W. G., Brighenti F., 2003, ARA&A, 41, 191
Meisenheimer K., 2003, New Astron. Rev., 47, 495
Mizuno Y., Hardee P., Nishikawa K., 2007, ApJ, 662, 835
Mizuno Y., Lyubarsky Y., Nishikawa K.-I., Hardee P. E., 2012, ApJ, 757, 16
Moll R., Spruit H. C., Obergaulinger M., 2008, A&A, 492, 621
Nalewajko K., Sikora M., 2009, MNRAS, 392, 1205
Narayan R., Li J., Tchekhovskoy A., 2009, ApJ, 697, 1681
O'Neill S. M., Beckwith K., Begelman M. C., 2012, MNRAS, 422, 1436
O'Sullivan E., Forbes D. A., Ponman T. J., 2001, MNRAS, 328, 461
Owen F. N., Ledlow M. J., 1994, in Bicknell G. V., Dopita M. A., Quinn P. J., eds, ASP Conf. Ser. Vol. 54, The First Stromlo Symposium: The Physics of Active Galaxies. Astron. Soc. Pac., San Francisco, p. 319
Owen F. N., Hardee P. E., Bignell R. C., 1980, ApJ, 239, L11
Owen F. N., Hardee P. E., Cornwell T. J., 1989, ApJ, 340, 698
Panaitescu A., Kumar P., 2002, ApJ, 571, 779
Perucho M., 2012, Int. J. Modern Phys. Conf. Ser., 8, 241
Phinney E. S., 1983, PhD thesis, Cambridge University
Porth O., 2013, MNRAS, 429, 2482
Porth O., Xia C., Hendrix T., Moschou S. P., Keppens R., 2014, ApJS, 214, 4
Ray T., 2012, EAS Publ. Ser., 58, 105
Rosen A., Hardee P. E., 2000, ApJ, 542, 750
Sanders R. H., 1983, ApJ, 266, 73
Scheuer P. A. G., 1982, in Heeschen D. S., Wade C. M., eds, Proc. IAU Symp. 97, Extragalactic Radio Sources. Reidel, Dordrecht, p. 163
Shakura N. I., Sunyaev R. A., 1973, A&A, 24, 337
Sikora M., Begelman M. C., Madejski G. M., Lasota J.-P., 2005, ApJ, 625, 72
Sironi L., Spitkovsky A., 2009, ApJ, 698, 1523
Sironi L., Spitkovsky A., 2011, ApJ, 726, 75
Sironi L., Spitkovsky A., 2014, ApJ, 783, L21
Sironi L., Petropoulou M., Giannios D., 2015, MNRAS, 450, 183
Spruit H. C., Daigne F., Drenkhahn G., 2001, A&A, 369, 694
Stawarz Ł., Ostrowski M., 2002, ApJ, 578, 763
Terlevich R., Davies R. L., Faber S. M., Burstein D., 1981, MNRAS, 196, 381
Trinchieri G., Fabbiano G., Canizares C. R., 1986, ApJ, 310, 637
Venturi T., Castaldini C., Cotton W. D., Feretti L., Giovannini G., Lara L., Marcaide J. M., Wehrle A. E., 1995, ApJ, 454, 735
Vlahakis N., Königl A., 2004, ApJ, 605, 656
Zakamska N. L., Begelman M. C., Blandford R. D., 2008, ApJ, 679, 990

This paper has been typeset from a TEX/LATEX file prepared by the author.